

**Effects of Mechanical Coupling on Oscillator Frequency
in a Micromechanical Accelerometer**

by

Kara Susanne Meredith

Submitted to the Department of Mechanical Engineering
in partial fulfillment of the requirements for the degree of
Bachelor of Science in Mechanical Engineering

and

Master of Science in Mechanical Engineering

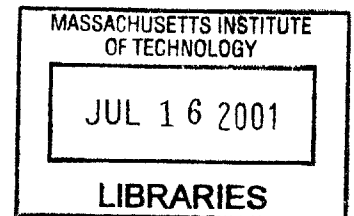
at the

MASSACHUSETTS INSTITUTE OF TECHNOLOGY

May 2001

© 2001 Kara Susanne Meredith. All rights reserved.

BARKER



The author hereby grants to MIT permission to reproduce and to distribute publicly paper and
electronic copies of this thesis document in whole or in part.

Author.....
Department of Mechanical Engineering
May, 2001

Certified by.....
Bernard Antkowiak
The Charles Stark Draper Laboratory, Inc.
Thesis Supervisor

Certified by.....
Rohan Abeyaratne
Professor
Thesis Supervisor

Accepted by.....
Ain A. Sonin
Chairman, Committee on Graduate Studies

This page intentionally left blank.



**Effects of Mechanical Coupling on Oscillator Frequency
in a Micromechanical Accelerometer**

by

Kara Susanne Meredith

Submitted to the Department of Mechanical Engineering
on May, 2001, in partial fulfillment of the
requirements for the degrees of
Bachelor of Science in Mechanical Engineering
and
Master of Science in Mechanical Engineering

Abstract

This thesis presents an analysis of the effect of mechanical coupling on the frequency behavior of the two oscillators in the SOA-3 micromechanical accelerometer. It also investigates the possible effect of the input acceleration on the degree of this mechanical coupling. A sensitivity study is also done to assess the dependence of the degree of mechanical coupling on the geometry of the beams that form the proof mass support system.

By doing a modal analysis using both a Finite Element and a mass-spring model of the accelerometer, it is shown that mechanical coupling does exist between the two oscillators, and is a function of the input acceleration on the device. It is also shown that the effects of mechanical coupling on the frequencies of the oscillators are the greatest at the input acceleration where the oscillator's frequencies, if completely uncoupled, would approach the same value. Finally, several design changes are suggested that reduce the amount of mechanical coupling between the oscillators.

Thesis Supervisor: Rohan Abeyaratne
Title: Professor

Thesis Supervisor: Bernard Antkowiak
Title: Draper Laboratory

This page intentionally left blank.

Acknowledgments

This thesis was prepared at The Charles Stark Draper Laboratory, Inc. under its Internal Research and Development (IR&D) program entitled Boost Analysis and Test. Publication of this thesis does not constitute the approval by Draper or the sponsoring agency of the findings or conclusions contained herein. It is published for the exchange and stimulation of ideas.

Author.....*Kara S. Mordill*.....

I would like to thank all of the people at Draper Laboratory and at MIT who helped me so much on this project. I am especially grateful to Bernie Antkowiak, Dr. Fred Nelson and Peter Sebelius who gave me an enormous amount of guidance in every stage of this project. I would also like to thank Dr. Rohan Abeyaratne for his advice and attention to this project, even though it was from far away. Thanks to Peter Sebelius and Ralph Hopkins for giving me this project and to Amy Duwel for all of our discussions of my results. Thanks to Bobby Dyer for helping me make the figures for this thesis. Thanks to Raj, Gary, Dave, Carissa and Kyrillian for making graduate school so interesting and fun.

Finally, I want to thank my wonderful family and friends, who gave me so much advice and encouragement. Mom and Dad, thank you for all of your help.

Assignment

Draper Laboratory Report Number T-1407

In consideration for the research opportunity and permission to prepare my thesis by and at The Charles Stark Draper Laboratory, Inc., I hereby assign my copyright of the thesis to the Charles Stark Draper Laboratory, Inc., in Cambridge Massachusetts.

Author.....

Kara Susanne Meredith

Table of Contents

1 INTRODUCTION	12
<hr/>	
2 BACKGROUND INFORMATION ON THE SOA-3	17
2.1 THEORY OF VIBRATING BEAM ACCELEROMETERS	17
2.2 DESIGN AND FABRICATION OF SOA-3	20
2.3 OPERATION OF SOA-3	22
2.4 MECHANICAL COUPLING	23
2.5 SIMULATION MODEL	24
<hr/>	
3 FINITE ELEMENT MODEL	28
3.1 PURPOSE OF FINITE ELEMENT MODEL	28
3.2 MODEL SPECIFICATIONS	28
3.3 MATERIAL PROPERTIES:	29
3.4 CONSTRAINTS	30
3.5 EQUAL OSCILLATORS VS. UNEQUAL OSCILLATORS	30
3.6 ANALYSIS USING THE FINITE ELEMENT MODEL	30
3.7 FINAL MODEL	32
<hr/>	
4 ANALYSIS	34

4.1	DEFINING COUPLING	34
4.1.1	APPLYING AN INERTIA LOAD	34
4.1.2	IMPORTANT MODE SHAPES	35
4.1.3	COUPLING RATIOS	36
4.2	COUPLING VS. GEOMETRY STUDY	39
4.2.1	STATIC ANALYSIS	40
4.2.2	MODAL ANALYSIS	41
4.3	MASS SPRING MODEL AND FREQUENCY ANALYSIS	41
5 RESULTS		47
<hr/>		
5.1	DEFINING COUPLING	47
5.1.1	FREQUENCIES FOR MODES 7 AND 8	47
5.1.2	COUPLING RATIO	49
5.2	COUPLING VS. GEOMETRY STUDY	52
5.2.1	BASE BEAM WIDTH:	52
5.2.2	FLEXURE WIDTH	54
5.2.3	LEVER ARM WIDTH	55
5.3	MASS SPRING MODEL AND FREQUENCY ANALYSIS	55
6 RECOMMENDATIONS AND CONCLUSIONS:		62
<hr/>		
APPENDIX A: OVERVIEW OF MODAL ANALYSIS		65
<hr/>		

List of Figures

FIGURE 1.1 SCHEMATIC OF SOA.....	14
FIGURE 1.2 OSCILLATOR FREQUENCIES AS A FUNCTION OF INERTIA LOAD.....	15
FIGURE 2.1 DEFORMED BEAM SHAPE.....	18
FIGURE 2.2 FLEXURE FREQUENCY AS A FUNCTION OF INERTIA LOAD.....	19
FIGURE 2.3 SCHEMATIC OF SOA-3.....	21
FIGURE 2.4 CAPACITIVE COMB DRIVE.....	22
FIGURE 2.5 SCHEMATIC OF OSCILLATORS WITH BLOCK PROOF MASS.....	24
FIGURE 2.6 BLOCK DIAGRAM OF SYSTEM SIMULATION.....	26
FIGURE 3.1 BEAM MODEL OF DEVICE FOR FINITE ELEMENTS.....	29
FIGURE 3.2 BEAM ELEMENT.....	31
FIGURE 3.3 FINAL FINITE ELEMENT MESH OF THE SOA-3.....	33
FIGURE 4.1 INERTIA LOAD ON THE FINITE ELEMENT MODEL OF THE DEVICE.....	35
FIGURE 4.2 NODES USED FOR OBSERVING CHANGES IN MODE SHAPE OF THE OSCILLATORS.....	37
FIGURE 4.3 OSCILLATORS DEFORMED IN THE SHAPE OF MODE 7.....	38
FIGURE 4.4 BEAMS WHOSE WIDTHS ARE CHANGES IN ITERATIONS DESCRIBED IN TABLE 5.1.....	40
FIGURE 4.5 FORCES ON OSCILLATOR FOR STATIC ANALYSIS.....	41
FIGURE 4.6 MASS SPRING MODEL OF THE SOA-3.....	42
FIGURE 5.1 FREQUENCIES OF MODES 7 AND 8 AS A FUNCTION OF INPUT ACCELERATION.....	48
FIGURE 5.2 FREQUENCIES FOR MODES 7 AND 8 AS A FUNCTION OF INPUT ACCELERATION NEAR THE FREQUENCY CROSSOVER POINT.....	49
FIGURE 5.3 COUPLING RATIO FOR MODES 7 AND 8 AS A FUNCTION OF ACCELERATION.....	50

FIGURE 5.4 COUPLING RATIO FOR MODES 7 AND 8 AS A FUNCTION OF INERTIA LOAD NEAR THE
FREQUENCY CROSS-OVER POINT. 51

FIGURE 5.5 COUPLING RATIOS FOR MODES 7 AND 8 FOR THE RANGE OF 0 TO .1 MICROG. 52

FIGURE 5.6 COUPLING AND INPUT AXIS MODE FREQUENCY AS A FUNCTION OF BASE BEAM WIDTH. 53

FIGURE 5.7 COUPLING AND INPUT AXIS MODE FREQUENCY AS A FUNCTION OF FLEXURE WIDTH. ... 54

FIGURE 5.8 COUPLING AND INPUT AXIS MODE FREQUENCY AS A FUNCTION OF LEVER ARM WIDTH.
..... 55

FIGURE 5.9 STIFFNESSES FOR OSCILLATOR AND COUPLING SPRINGS IN SECTION 5.3'S MASS SPRING
MODEL..... 56

FIGURE 5.10 OSCILLATOR FREQUENCY AS A FUNCTION OF INERTIA LOAD..... 57

FIGURE 5.11 OSCILLATOR FREQUENCY AS A FUNCTION OF ACCELERATION NEAR FREQUENCY
CROSSOVER POINT. 58

FIGURE 5.12 DEVICE READOUT AS A FUNCTION OF ACCELERATION..... 59

FIGURE 5.13 DEVICE READOUT AS A FUNCTION OF ACCELERATION NEAR THE FREQUENCY CROSS-
OVER POINT. 60

FIGURE 5.14 FREQUENCY READOUT ERROR AS A FUNCTION OF ACCELERATION..... 61

1 Introduction

With the increasingly stringent accuracy requirements in strategic guidance applications due to short flight times and high acceleration levels of vehicles, inertial guidance technology has evolved from large complex systems like the Pendulous Integrating Gyroscopic Accelerometer (PIGA) to the microelectromechanical (MEMS) accelerometers and gyroscopes that are used today. Because MEMS systems are less complex, less expensive and more easily fabricated than the more traditional inertial sensors, they have become a popular alternative. [3]

Draper Laboratory is currently developing the third generation of the Silicon Oscillating Accelerometer (SOA-3), which is a MEMS based sensor that will have the ability to achieve high performance. The SOA-3 is in the family of Vibrating Beam Accelerometers (VBAs), and measures the change in frequency of two mechanical oscillators under inertial loading from a large proof mass. While Vibrating Beam Accelerometers are typically fabricated from quartz and are larger than MEMS scale, the SOA is a silicon MEMS based device. There are several advantages to using the SOA over other Vibrating Beam Accelerometers. First, because the semiconductor grade silicon used in the device is a perfectly elastic material that can be produced with very low levels of impurities, they have higher performance capabilities and repeatability. Second, because MEMS devices are very small (millimeter scale) compared to the

traditional VBAs, the oscillators are isolated from stress effects in the packaging. Finally, the capacitive drive system for the oscillators allows for greater design flexibility than the piezoelectric quartz actuation. [3]

With the benefits of the sleek design of the MEMS SOA, there are also many design challenges faced in order to meet the performance requirements for strategic guidance applications. New fabrication techniques, thermal stability, and the electronics for the control system are all important to the success of the device. Another important issue that has come about in the design and testing of the device is that of mode locking.

Figure 1.1 below shows a schematic of the basic operation of the SOA. There is a large proof mass that is attached on both sides to a flexible beam oscillator (beam1 and beam 2) whose opposite end is fixed. When the proof mass experiences an acceleration, a in the direction of the input axis, it develops an inertial force, F . The force F on the proof mass puts Beam 1 into compression by a force F_1 and Beam 2 into tension by a force F_2 . Forces F_1 and F_2 add together to equal the inertia force, F , on the proof mass.

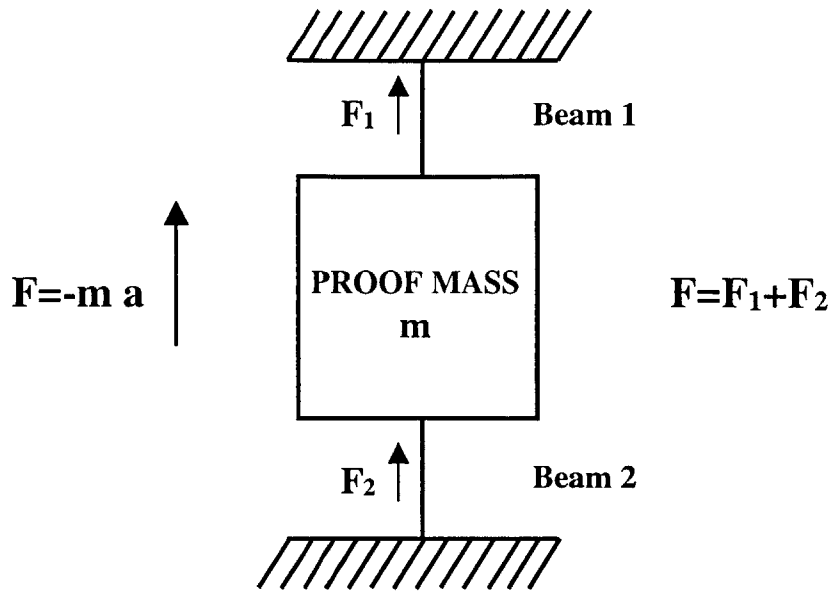


Figure 1.1 Schematic of SOA.

When the beams are allowed to oscillate laterally, the beam in compression will oscillate at a lower frequency as the input acceleration increases and the beam in tension will oscillate at a higher frequency. The beam acts like a string held taut that will vibrate quickly when plucked but when the tension is released, it will vibrate more slowly. The inertia load (hence the acceleration) on the device is measured by taking the difference between the frequencies (called the “frequency readout”) of Beam 1 and Beam 2 and multiplying that difference by a scale factor. Because the frequency of one of the oscillators is increasing and the other is decreasing, their frequency paths will cross at a particular inertia load. This is called the frequency cross over point.

If the two oscillators are completely uncoupled, and the frequencies of the two oscillators observed over an increasing inertia load on the proof mass, their paths would look like the solid line in Figure 1.2 below. The uncoupled oscillator frequencies are determined using fixed-fixed beam equations.[11] In this case, the frequencies of the oscillators change with inertia load and

the scale factor is the slope of the line. This curve is non-linear but becomes more linear at higher frequencies.

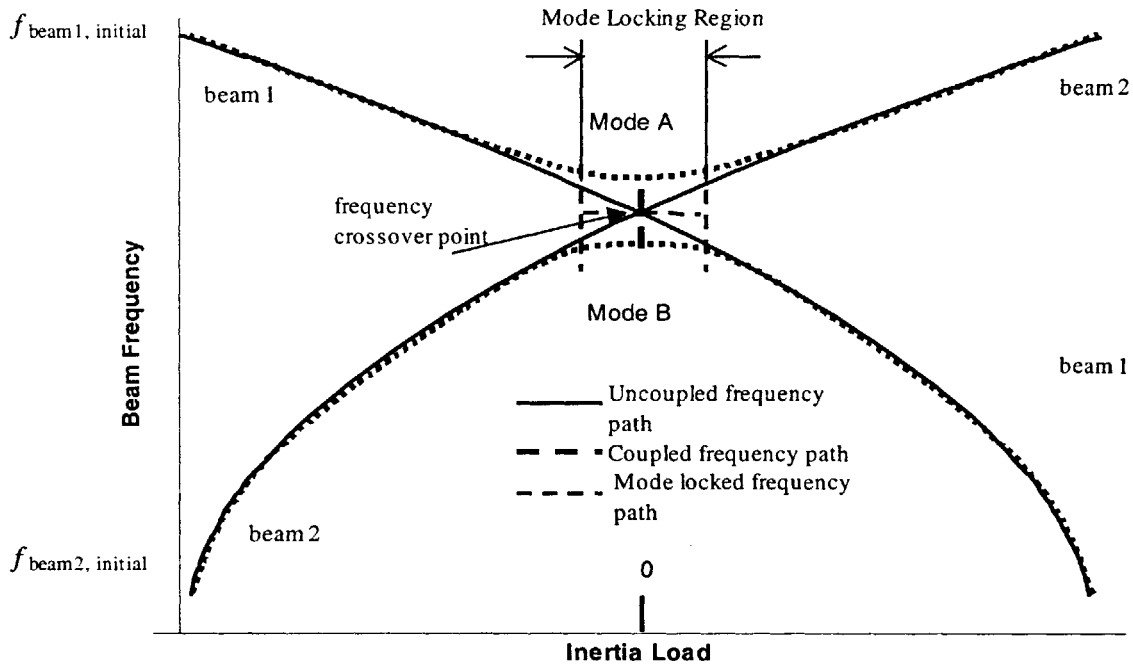


Figure 1.2 Oscillator frequencies as a function of inertia load.

If the oscillators are coupled together, the frequencies for the modes of oscillation for the two oscillators over an increasing inertia load would look like the dotted lines in Figure 1.2. Beam 1's frequency first follows Mode A and at the frequency crossover point becomes Mode B (represented by the dark dotted line in Figure 1.2). The opposite is true for Beam 2. The difference in frequency of the dotted line to the solid line is a result of mode coupling. If the oscillators vibrate at the same frequency as shown by the dashed line in Figure 1.2 above, this is called the mode locking. Coupling between the oscillators is one of the elements that must be present for mode locking to occur. The range of values for inertia load over which they are

locked is the mode locking region. The frequencies will eventually separate with increased inertia load and continue on their original paths.

As seen in Figure 1.2 both coupling and mode locking cause a deviation in the frequency readout of the device (the difference between the two oscillator frequencies at a particular inertia load) with respect to the uncoupled case. If left uncompensated, the coupling between the oscillators would result in an error in the predicted acceleration. Furthermore, within the region of mode locking, the readout of the device is zero.

In this study, a finite element model of the SOA-3 is created to determine the mode shapes for the device and the frequency ranges for those modes as a function of the input acceleration/inertia load. Coupling between the two oscillators is defined and quantified both as a function of input acceleration and the geometry of the device. Most importantly, from the information gained from these models, the effect of mechanical coupling on the frequencies of the oscillators is determined.

2 Background Information on the SOA-3

The SOA is in the family of the vibrating beam accelerometer, which can be represented as a large mass connected on either side to two flexible beams. On the opposite ends, the beams are fixed, as shown in Figure 2.1. The beams are labeled beam 1 and beam 2 and the large mass is M . The flexible beams are much smaller in size and mass than the large mass that connects them.

2.1 Theory of Vibrating Beam Accelerometers

Because the beams are fixed on one end they cannot move in the y -direction but they are allowed to vibrate laterally in the x -direction. Figure 2.1 also shows a deformed shape when the beams are vibrating.

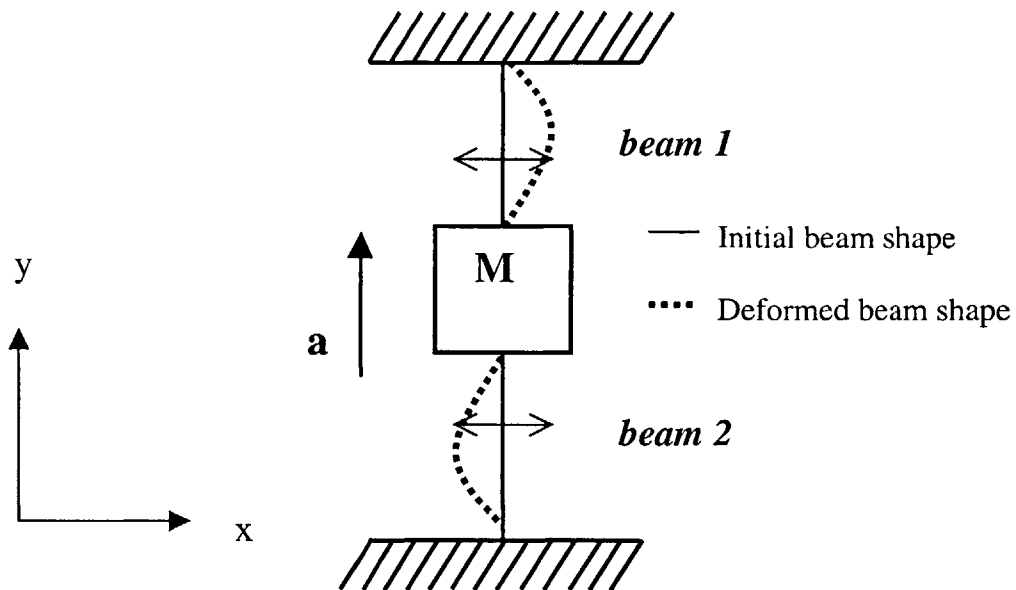


Figure 2.1 Deformed beam shape.

If the mass experiences an input acceleration and thus an inertia load in the positive y -direction, it puts a force on both of the beams in the axial direction. Beam 1 goes into compression and beam 2 goes into tension. Now, when the beams are vibrated laterally, the frequency of vibration for beam 1 will decrease due to the compressive force and the frequency of beam 2 will increase because of the tensile force. In the absence of coupling, identical beams will vibrate at the same frequency when the inertia load is zero. As the inertia load on the mass increases, the frequency of beam 1, f_1 decreases and the frequency of beam 2, f_2 increases. For small changes in the inertia load around zero, the change in frequency of the beams to inertia is nearly linear as shown in Figure 2.2.

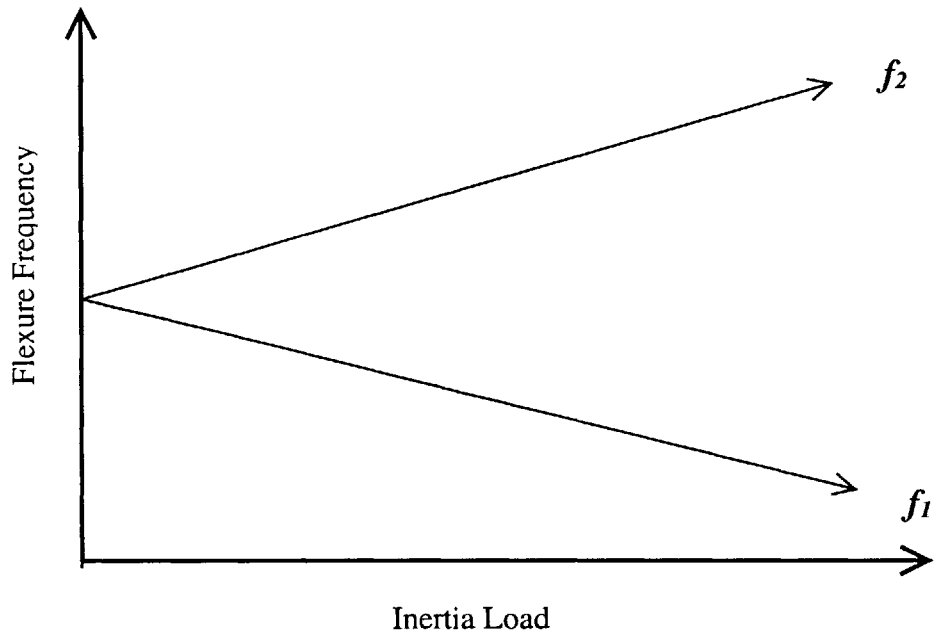


Figure 2.2 Flexure frequency as a function of inertia load.

The difference in the frequencies of each of the flexures is proportional to the acceleration because the frequencies of the two flexures change with acceleration. The change in frequency divided by the acceleration of gravity, g ($g= 9.8 \text{ m/s}^2$), is defined as the scale factor.

$$SF = \frac{(f_1 - f_2)}{g} \tag{2.1}$$

$$g = \frac{1}{SF}(f_1 - f_2) \tag{2.2}$$

2.2 Design and Fabrication of SOA-3

The SOA-3 is a MEMS structure fabricated from single crystal silicon[3]. It consists of a large proof mass and two oscillators on opposite sides of the device, etched from silicon. Figure 2.4 below is a schematic of the SOA-3 design. The silicon is attached to a Hoya glass substrate via bond pads. The thermal properties of Hoya glass are similar to silicon. The proof mass movement is restricted in all directions except the input axis direction, which is along the y-axis.

Both of the oscillators are configured in a “tuning fork” design. Each oscillator consists of two flexible beams or flexures with a small comb-tooth mass at the center of the beam. Both of the flexures on each oscillator are identical in size and mass. The flexures are attached at both ends to a base beam, which is wider and stiffer than the flexures. One of the base beams is attached to the glass substrate fixing it to the ground, while the other is attached to the proof mass via a lever arm as shown in Figure 2.3. The proof mass consists of the entire silicon structure aside from the oscillators and the bond pads. The proof mass exerts the inertia force on the base beams through the lever arm and the base beams then exert that force onto the flexures. The lever arm multiplies the force exerted on the oscillators and allows the actual size of the proof mass to be smaller for the same scale factor.

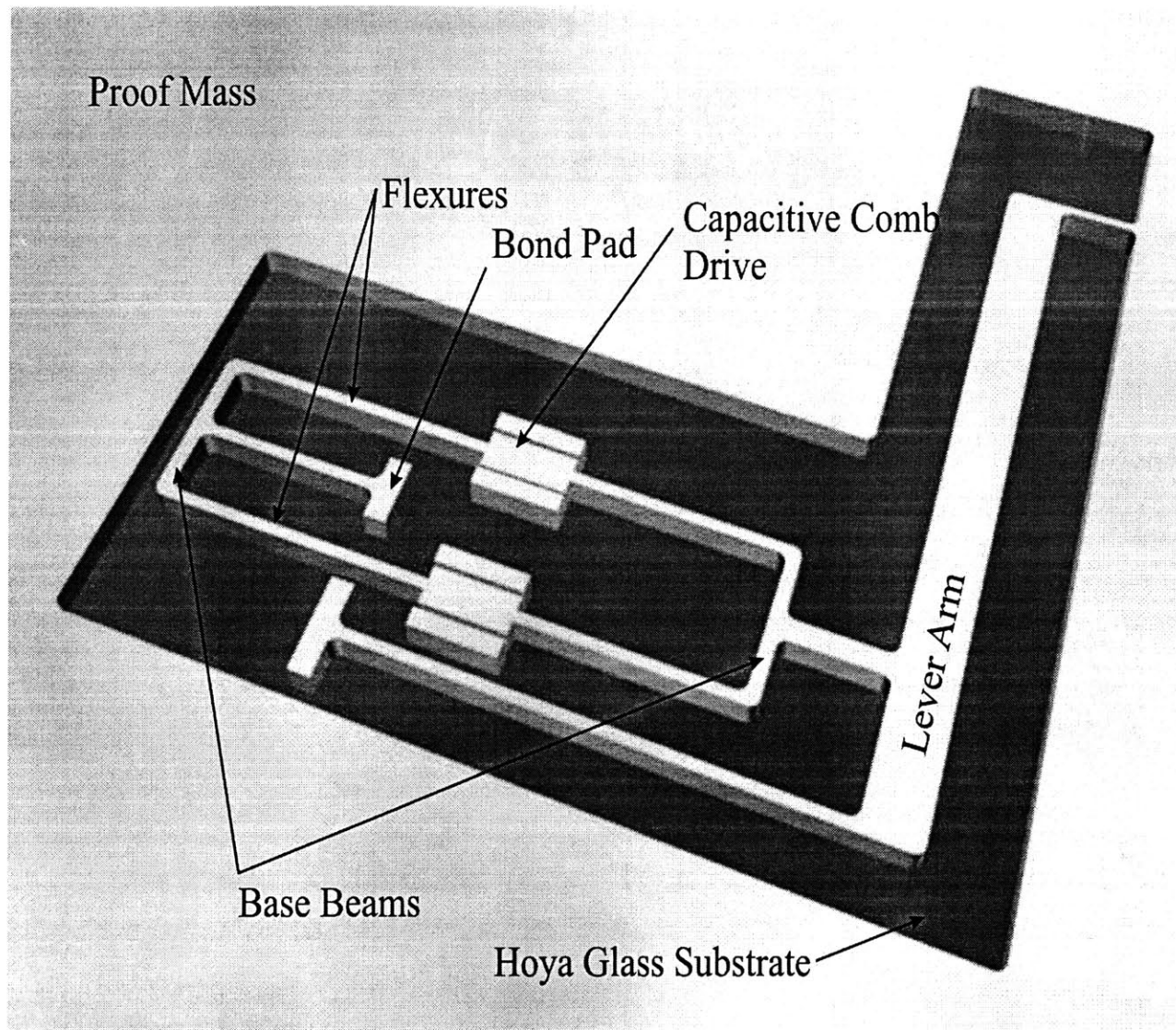


Figure 2.3 Schematic of SOA-3.

The scale factor for this device is designed to be large so that small changes in inertia load can be resolved. There are two oscillators rather than one to eliminate the effect of common disturbances such as creep and temperature changes. For example, the silicon material has a modulus temperature sensitivity of -50 to -100 ppm/ $^{\circ}\text{C}$ [9] so, if there were one oscillator, the temperature change would effect the frequency. The two oscillator design is beneficial because both oscillators experience the same temperature change and they both would increase or

decrease in frequency by the same amount due to temperature. When the frequency difference is calculated between the two, the temperature effect is eliminated.

2.3 Operation of SOA-3

During operation, the oscillators are driven at their resonant or “bias” frequency. Because their resonant frequencies change with acceleration, there is a mechanism that senses the resonant frequency and feeds the information back to the drive mechanism. The oscillators are driven using a capacitive comb drive. Figure 2.4 shows an enlarged drawing of the capacitive comb drive.

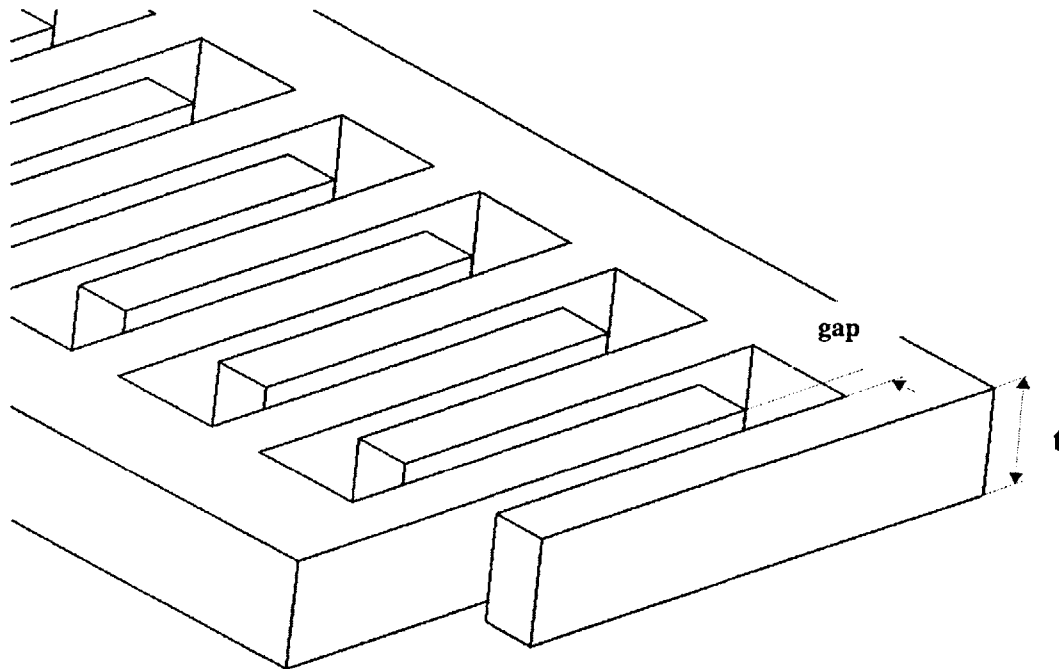


Figure 2.4 Capacitive Comb Drive.

The inner comb fingers are part of the flexure and are located in the center on both sides of the flexure beam. The flexures and comb fingers are etched from the same silicon piece. On each side of the flexure are comb fingers anchored to the hoyo glass substrate and etched from

silicon. On the outer side of the oscillator the comb fingers are the drive mechanism and on the inside of the oscillator the comb fingers are the sensing mechanism. The outer and inner combs each intermesh with the comb fingers on their side of the flexure, creating parallel plate capacitors. Motion is driven using electrostatic force, F_{el}

$$F_{el} = \frac{1}{2} V^2 \frac{\epsilon_0 t}{gap}. \quad 2.3$$

V is the voltage across the capacitor, t is the thickness of the silicon device in the z -direction, gap is the width of the gap between the comb fingers and ϵ_0 is the permittivity of free space. The change in capacitance of the sensing mechanism due to changes in the amplitude of the oscillations is then measured and converted to a frequency and fed back to the drive mechanism.[9] The readout from the device also comes from the sensing mechanism. It is obtained by taking the difference in frequency between the two oscillators.

2.4 Mechanical Coupling

There are two types of coupling that can exist in the accelerometer, mechanical and electrical. The electrical coupling in the SOA-3 is anticipated to be small; therefore the focus of this study is on mechanical coupling. Mechanical coupling occurs in the SOA-3 because one oscillator's motion influences the other oscillator through the proof mass. Although the proof mass is several orders of magnitude more massive than the oscillators, because the proof mass is flexible and moves, it affects the motion of the oscillators. Figure 2.5 shows a possible mechanism for coupling between the SOA-3 oscillators through the motion of the proof mass.

This schematic gives intuition about how one oscillator might react to the motion of the other, due to the motion of the proof mass. If oscillator 1's flexures are bowed in towards each

other and its base beams are pushed out, it pushes the proof mass away from it towards the other oscillator. This push on the proof mass causes the base beams on oscillator 2 to bow in and its

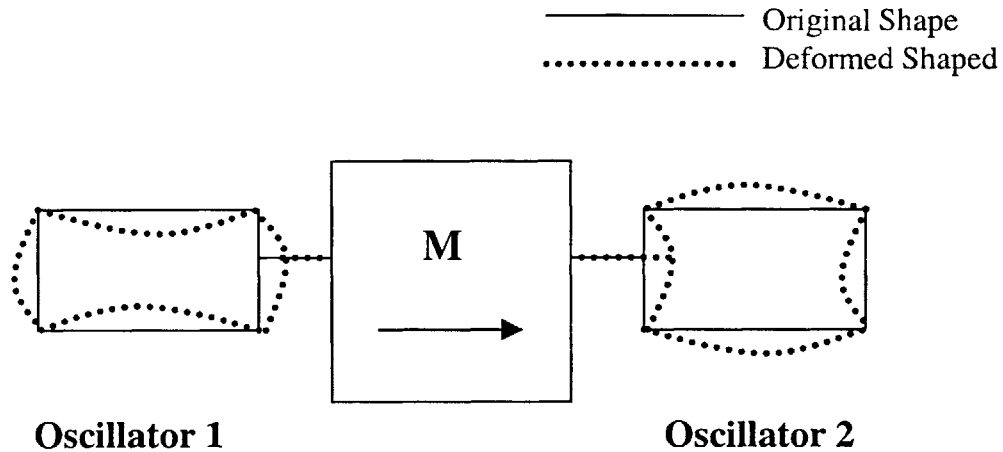


Figure 2.5 Schematic of oscillators with block proof mass.

flexures to bow away from each other. Of course, on the device these reactions are small. But the motion of one oscillator does affect the other via the movement and flexibility of the proof mass. This effect is the coupling between the two oscillators.

2.5 Simulation Model

The model described in this section will eventually be used to determine the effects of a time-varying inertia load on the SOA-3 and is the motivation for the coupling analysis described in the following sections. This model will be used after the effects of mechanical coupling on the frequency readout for the device are and expressed in a time domain plant model.

The development of this plant model can be shown by expressing the SOA-3 equations of motion in physical coordinates as:

$$[M]\{\ddot{x}\} + [C]\{\dot{x}\} + [K]\{x\} = \{F_{el}\}, \quad 2.6$$

where $[M]$ and $[K]$ are the mass and stiffness matrices respectively and C is the system damping, obtained from a finite element model of the system; and $\{F_{el}\}$ is not the inertia force rather it is the force that drives the oscillators in a specific mode. By solving for the eigenvalues and eigenvectors of the system, the modes of interest(see Appendix B): the input axis mode, the hula modes and the drive modes, can be identified. The eigenvalues and eigenvectors that are associated with those modes can then be used to change the system from physical to modal coordinates. If $[\Psi]$ is the matrix of eigenvectors, the following relationship between physical and modal coordinates is true:

$$\{x\} = [\Psi]\{q\} \quad 2.7$$

where q is the set of modal coordinates. Substituting Equation 2.7 into Equation 2.6 and premultiplying Ψ^T , the equation of motion in terms of modal coordinates becomes:

$$[\Psi^T][M][\Psi]\{\ddot{q}\} + [\Psi^T][C][\Psi]\{\dot{q}\} + [\Psi^T][K][\Psi]\{q\} = [\Psi^T]\{F_{el}\} \quad 2.8$$

where

$$[\Psi^T][M][\Psi] = [I] \quad 2.9$$

$$[\Psi^T][C][\Psi] = \begin{bmatrix} \cdot & & \\ & 2\xi\omega_n & \\ & & \cdot \end{bmatrix} \quad 2.10$$

$$[\Psi^T][K][\Psi] = \begin{bmatrix} \cdot & & \\ & \omega_n^2 & \\ & & \cdot \end{bmatrix}. \quad 2.11$$

The damping is estimated to be $2\zeta\omega_n$ where ζ is the damping ratio and ω_n is the natural frequency. The equation of motion that will go into the simulation is:

$$\{\ddot{q}\} = [\Psi^T] \{F_{el}\} - \begin{bmatrix} \cdot & & \\ & 2\zeta\omega_n & \\ & & \cdot \end{bmatrix} \{\dot{q}\} - \begin{bmatrix} \cdot & & \\ & \omega_n^2 & \\ & & \cdot \end{bmatrix} \{q\}. \quad 2.12$$

This shows that there are n independent equations of motion. By the method of modal superposition the modes of interest can be extracted. Now the simulation contains only the modes of interest. A block diagram of the system is shown in Figure 2.6 below.

In order to incorporate inertia load into the system, ω_n is made into a function of F :

$$\omega_n = \frac{n^2\pi^2}{l^2} \sqrt{\left(\frac{EI}{\rho A}\right)\left(1 + \frac{Fl^2}{n^2\pi^2 EI}\right)} \quad 2.13$$

where n is the mode number, l is the length of the beam elements, E is Young's Modulus, ρ is the density, A is the cross sectional area of the beams, and F is the inertia load. Now, using this simulation, an inertia load can be applied at any rate, like a ramp or a step function.

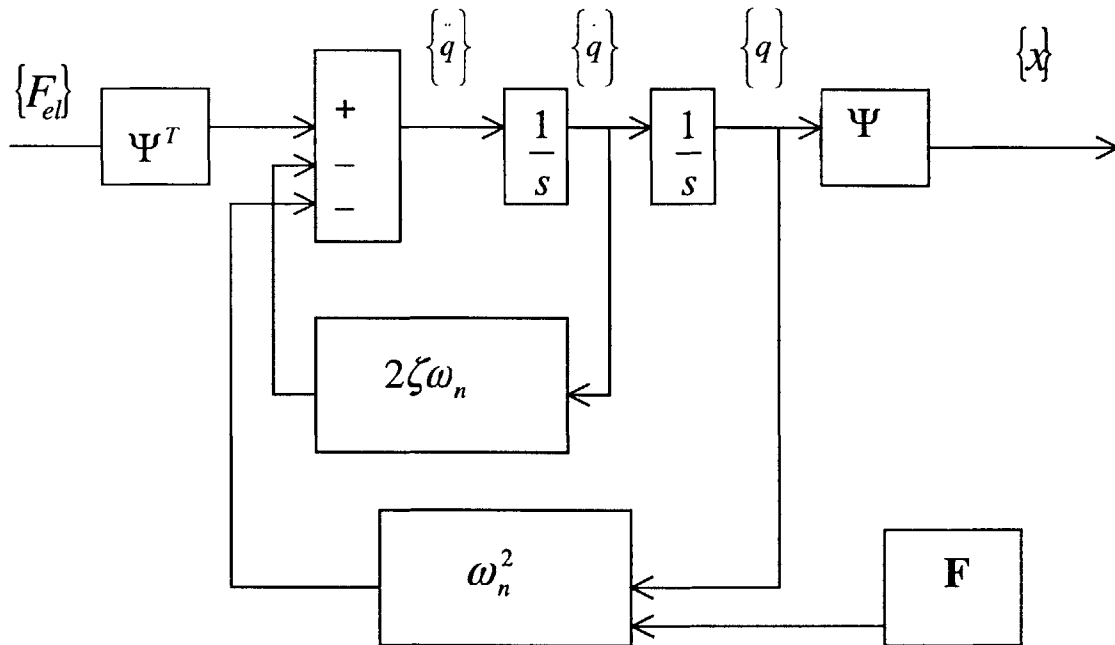


Figure 2.6 Block diagram of system simulation.

This model now includes a basic coupling as part of the eigenvectors. It includes the effect of inertial loads on the eigenvalues per equation 2.13. However, the effect of inertial loading on the eigenvectors is not included. In this sense the effect of inertial loading on the coupling is not included. This topic will be investigated in the following sections.

3 Finite Element Model

3.1 Purpose of Finite Element Model

Finite element model of the SOA were created using Nastran [5] and Ansys[1] in order to model the SOA-3. The finite element models then can be used for several types of analysis, like static and modal analyses. The geometry of the device can be specified, as can the material properties, the constraints and external forces. These properties can easily be changed for specific analyses.

3.2 Model Specifications

Because the oscillators are flexible beams, a beam model was chosen as an accurate representation of the device. Figure 3.1 shows the beam model of the device. Beams 1-4 represent the proof mass connections to the glass substrate. Beams 5,6 and 7 represent the lever arm on one oscillator with 8 as a connection to the substrate; and beams 19,20 and 21 are the lever arm for the other with a connection to the glass substrate by 23. Oscillator 1 is represented by beam elements 9, 10, 16, 17 which constitute the base beams; beam elements 12, 13, 14, 15 represent the flexures; and 11 and 18-the connections to the lever arm and substrate respectively. A small concentrated mass is placed between elements 12 and 14 and between elements 13 and

15 to represent the capacitive comb drives. Similarly, oscillator 2 is represented by beam elements 24, 25, 30, 31- the base beams; beam elements 26, 27, 28, 29-the flexures; and 22 and 32 are the connections to the lever arm and substrate respectively. Concentrated masses (black rectangles) representing the comb drives are placed between elements 26 and 28 and between elements 27 and 29 to represent the capacitive comb drives. Here the proof mass is represented by a rigid body element (the black square) connecting the free ends of elements 1-4 and the lever arms, elements 5 and 19 and concentrated in the middle of the two oscillators.

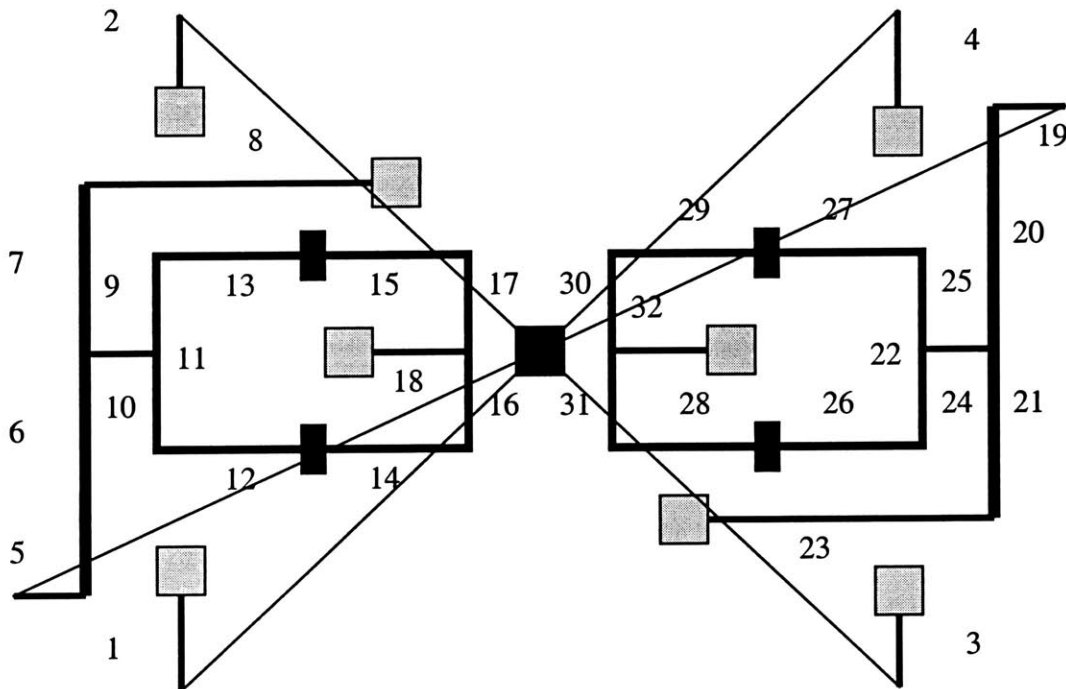


Figure 3.1 Beam model of device for finite elements.

3.3 Material Properties:

Single crystal silicon is an anisotropic cubic material. For ease of analysis isotropic properties were used. The elements were given the following material properties [9]:

Young's Modulus:

$$E = 1.7 * 10^{11} \frac{N}{m^2} = 170 \frac{GN}{m^2}$$

Poisson's Ratio:

$$\nu = .3$$

Density:

$$\rho = 2330 \frac{kg}{m^3}$$

Shear Modulus:

$$G = \frac{E}{2(1+\nu)} = 0.654 \times 10^{11} \frac{N}{m^2} = 65.4 \frac{GN}{m^2}.$$

3.4 Constraints

In Figure 3.1 the gray boxes represent the bond pads on the ends of the beam elements, meaning that they are not allowed to move in any of the six degrees of freedom.

3.5 Equal Oscillators vs. Unequal Oscillators

Oscillators which are identical in size are called "equal" and their frequencies cross at 0 g. The actual SOA-3 is designed so that the oscillators are slightly different in size so that their frequency crossover point is not at zero within +/- 5g. Although this is detrimental to performance discussed in section 2.2, this eliminates any coupling or mode locking issues in the 1 g gravitational testing. If the cross sectional areas of the flexures on each of the oscillators are different, they will vibrate at different frequencies in the absence of an inertia load. The difference in geometry can be accounted in the finite element model by calculating their area moments of inertia.

3.6 Analysis Using the Finite Element Model

Both static and dynamic analyses were done using this model. A static analysis will show how much one oscillator moves with respect to the other when a static load is applied. A dynamic analysis gives the eigenvalues (natural frequencies) of a system and the eigenvectors

(mode shapes) associated with each of those eigenvalues. A system vibrates at a natural frequency when it elastically deformed and then released. The restoring strain energy causes it to vibrate in a periodic motion about its equilibrium point. [2]

The first step in a dynamic analysis is to create the mass and stiffness matrices for the model. Each beam element in the model has an elemental mass matrix m_e , which are combined into one large mass matrix M for the entire system. The elemental mass matrix [2] for the beam element in Figure 3.2 is

$$m_e = \frac{\rho A_e l_e}{420} \begin{bmatrix} 156 & 22l_e & 54 & -13l_e \\ & 4l_e^2 & -13l_e & -3l_e^2 \\ \text{symmetric} & & 156 & -22l_e \\ & & & 4l_e^2 \end{bmatrix} \quad 4.1$$

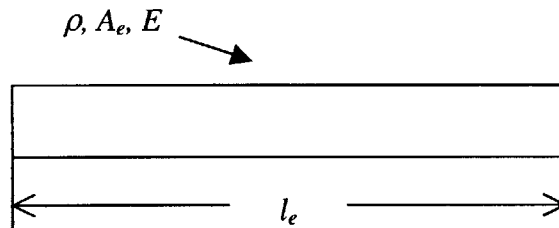


Figure 3.2 Beam element.

Each beam element in the model also has an elemental stiffness matrix k_e . The element stiffness matrices are combined into one large stiffness matrix K for the entire system. The elemental stiffness matrix [2] for the beam element in Figure 3.2 is

$$k_e = \frac{EI}{l_e^3} \begin{bmatrix} 12 & 6l_e & -12 & 6l_e \\ & 4l_e^2 & -6l_e & 2l_e^2 \\ \text{symmetric} & & 12 & -6l_e \\ & & & 4l_e^2 \end{bmatrix} \quad 4.2$$

$[K]$ and $[M]$ are both symmetric and positive definite.

Next $[K]$ and $[M]$ are used to obtain the eigenvalues and eigenvectors for the system using modal analysis (See Appendix 1). $[K]$ and $[M]$ make up the equations of motion for the unforced system when they are in the form:

$$[K]U_i = \lambda[M]U_i \quad i = 1 \dots n \quad 4.3$$

where n is the number of degrees of freedom for the system, λ_i are the eigenvalues for the system which are the natural frequencies squared. U_i are the corresponding eigenvectors. The eigenvalues and eigenvectors are obtained by finding a characteristic polynomial in terms of λ :

$$([K] - \lambda_i[M])U_i = 0 \quad 4.4$$

$$\det([K] - \lambda_i[M]) = 0. \quad 4.5$$

Once the polynomial is solved for λ_i , and then for each λ_i the eigenvector that satisfies Equation 4.4 is found.

3.7 Final Model

Finally, after using the model described above to gain intuition about the feasibility and accuracy of using beam elements to represent the oscillators, a correction was made to account for the flexibility of the proof mass using the shell/beam model of the SOA-3. The difference between the pure beam model and this model is that the proof mass and comb drives are represented by their geometry rather than as concentrated masses. This model was made by importing a solid model from ProEngineer.[8] It contains a mixed mesh of shell and beam

elements. Figure 3.3 below shows the finite element mesh for the final model. Also, to make analysis easier, in the final model the oscillators are equal in size so that their frequency crossover point will be at zero inertia load, which is different than the actual device.

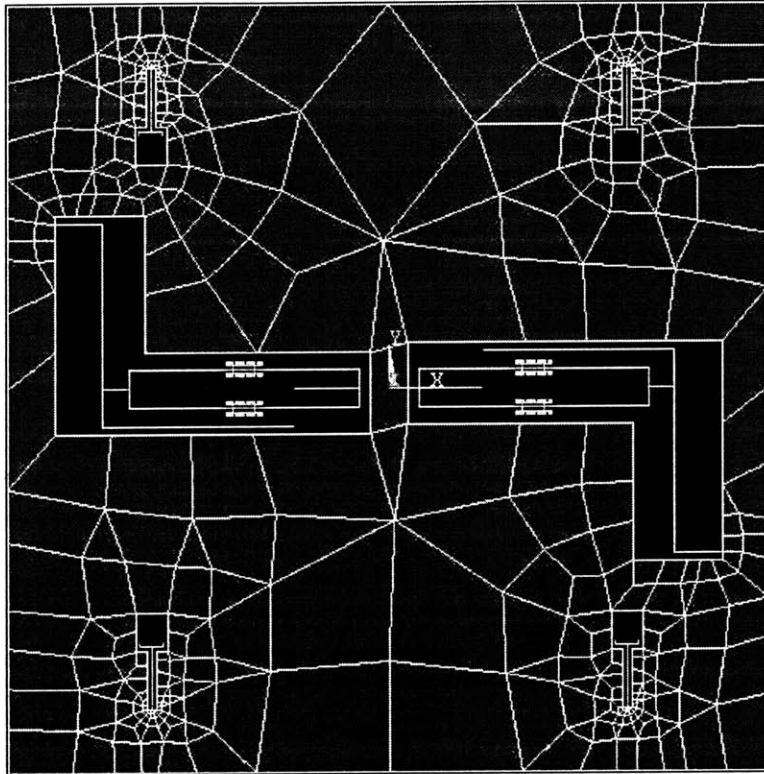


Figure 3.3 Final finite element mesh of the SOA-3.

In shell elements there is no in-plane rotational stiffness at the nodes. To determine the impact of joining beam to shell elements at the lever arm to the proof mass, various test runs were made. Nodal constraints were added where the lever arm meets the proof mass on each of the oscillators. In the first analysis, no rotation was allowed at this node. In the next analyses, beam elements were added connecting the end of the lever arm node to surrounding nodes in the proof mass. In both cases, the coupling between the oscillators increased by adding the constraints. The unconstrained case is used in this analysis. Further investigation is required to precisely model the lever arm to proof mass junction.

4 Analysis

4.1 Defining Coupling

A complete model of the SOA system must include some information about the coupling of the system. It is important then, to define the coupling between the oscillators determine if it is a function of the inertia load on the device and quantify it so that the information can be used in a model of the system. Here the beam/plate Finite Element Model described in Section 3 shown in Figure 3.3 is used to obtain this information about the SOA-3.

4.1.1 Applying an Inertia Load

In order to determine the effects of a inertia load on the frequency of the oscillators, the mode shapes and the coupling between the two oscillators, an inertia load is applied to the model (using the program Ansys[1]). Figure 4.1 shows the inertia load applied to the meshed model of the SOA. It is applied along the y-axis, which is called the “input axis.” The white arrow in Figure 4.1 points to the right, which means the device is accelerating to the left. The inertia load is a force on the proof mass. The force on the proof mass then puts oscillator 1 on the left in tension and the oscillator 2 on the right in compression.

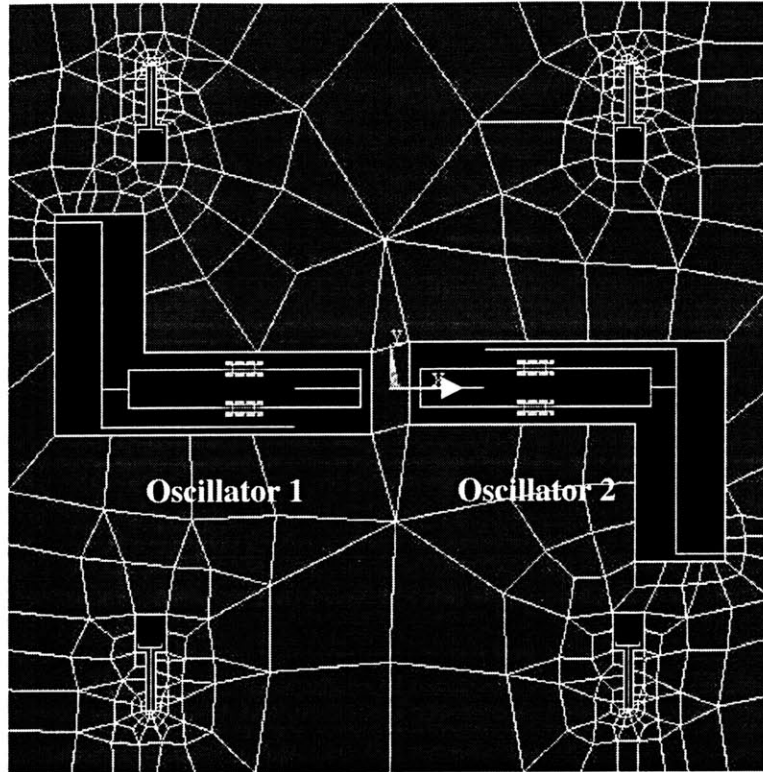


Figure 4.1 Inertia load on the finite element model of the device.

When the oscillators are equal, their frequency cross-over point is at 0 g. The range from 0g to 500 μ g is the region of potential mode locking so it is important to look at inertia loads very close to zero[4]. It is also important to apply much larger inertia loads to obtain the general trends caused by changing the inertia load on the oscillator. Thus, the acceleration associated with the inertia load is also varied from 0g to 5g. Only positive inertia loads are applied (i.e. only applied in the positive y-direction) because when the oscillators are equal, a negative inertia load will have an equal and opposite effect as a positive inertia load.

4.1.2 Important Mode Shapes

The mode shapes for the system are also obtained using the Finite Element model in Figure 3.3. The mode shapes are the eigenvectors that are associated with the system's eigenvalues. Appendix B shows the most important modes of the system. These modes are the

lowest frequency modes and more useful in operating the device than the higher frequency modes. The lowest frequency mode is called in “input axis mode,” and it involves only the movement of the proof mass in the input axis direction. Next there are several modes where the proof mass bends in the z -direction. The modes that involve only the movement of the oscillators are at a higher frequency than the modes of the proof mass. There are two modes that involve the oscillators moving together in the x -direction. These are called “hula modes.” Finally, there are the “drive modes” where the oscillators move opposite to each other in the x -direction. In each of these two drive modes, one of the oscillators has a very large displacement while the other has a very small displacement. As shown in Figure 4.3, the oscillators are driven in this “drive mode” shape. For the sake of this study, it is assumed that the drive modes and the input axis mode contribute the most toward the coupling of the two oscillators. From modal analysis, it is known that the input axis mode is “mode 1,” the lowest frequency mode and the drive modes are “mode 7” for oscillator 2 in compression and “mode 8” for oscillator 1 in tension.

First the inertia load is varied and the frequencies of Modes 7,8, and 1 are obtained. As the inertia load is varied it is also determined if these mode shapes change both over a broad range of inertia loads and near the frequency crossover point.

4.1.3 Coupling Ratios

Since modes 1, 7, and 8 contribute most to the coupling of the oscillators, observing their mode shapes can give a great deal of information. By picking corresponding nodes on each of the oscillators, as shown in Figure 4.2, and observing the displacement of those nodes with respect to their unloaded position, under varying G -loads, the appropriate information to describe

coupling is gathered. Figure 4.3 shows the deformed shape of Mode 7. In mode 7, oscillator 2 moves a great deal and oscillator 1 moves very little.

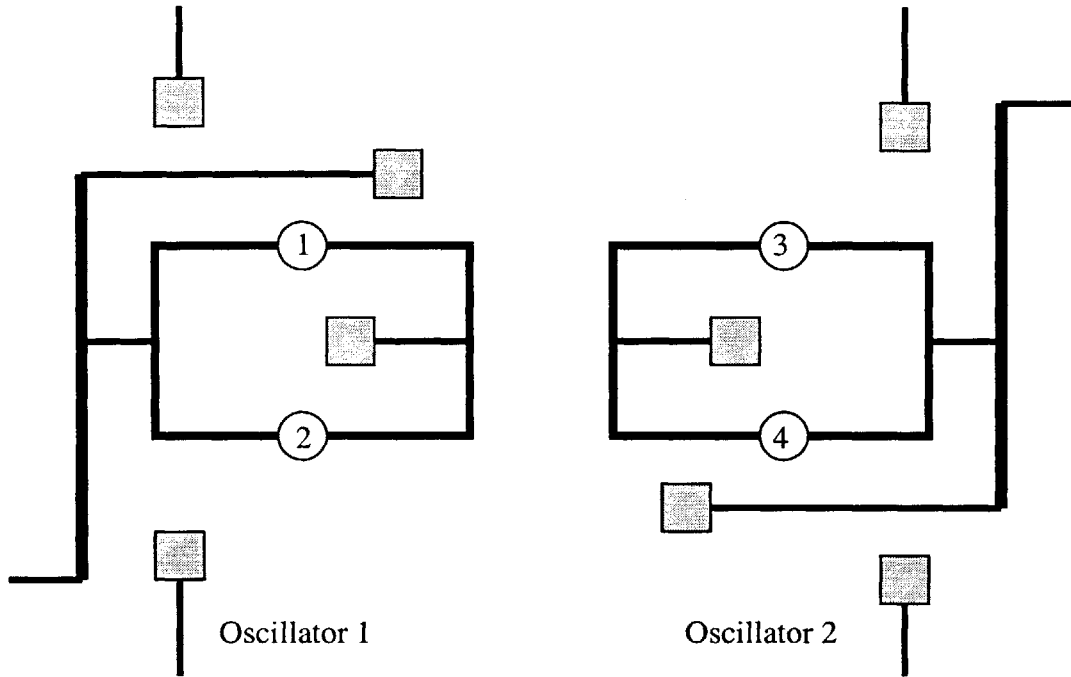


Figure 4.2 Nodes used for observing changes in mode shape of the oscillators.

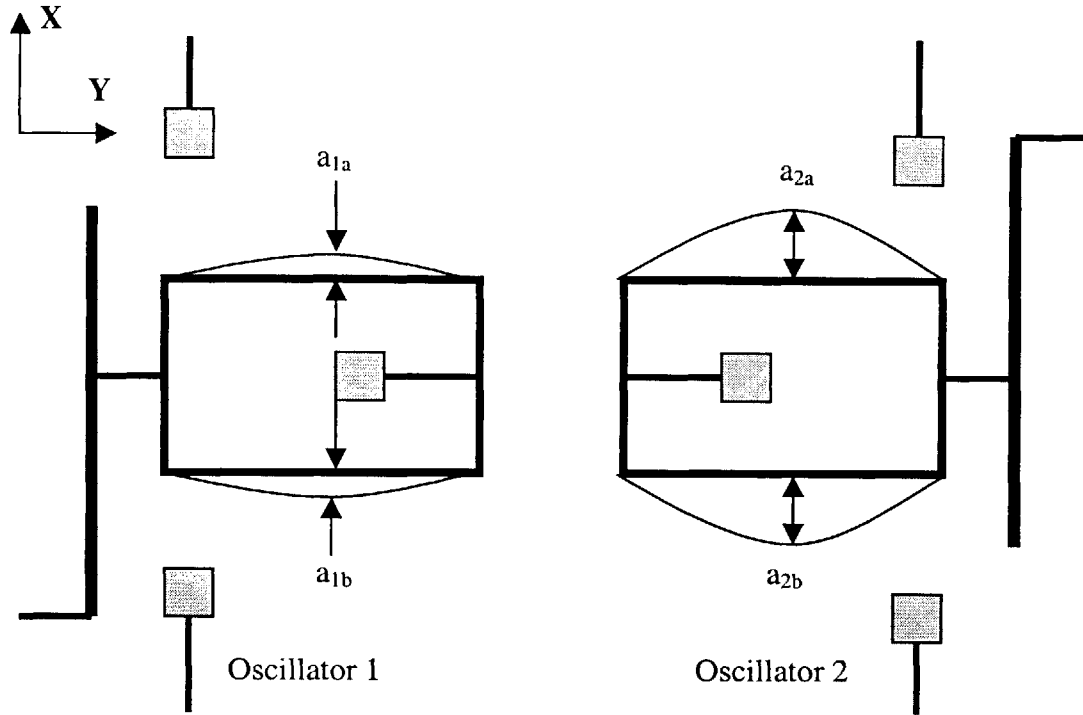


Figure 4.3 Oscillators deformed in the shape of mode 7.

In the figure a_{1a} and a_{1b} represent the large displacement (displacement of nodes 1 and 2) of one of the oscillators, a_{2a} and a_{2b} represent the small displacement (displacement of nodes 3 and 4). The values a_1 and a_2 are the average displacements in the x -direction of the flexures in oscillators 1 and 2 respectively and are calculate using the following formulas:

$$a_1 = \frac{|a_{1a}| + |a_{1b}|}{2} \quad 4.1$$

$$a_2 = \frac{|a_{2a}| + |a_{2b}|}{2} \quad 4.2$$

The ratio a_2/a_1 , large oscillator displacement/ small oscillator displacement, is defined as the coupling ratio for mode 7 and gives the most information about how the coupling of the oscillators change with G -load. As the ratio a_2/a_1 approaches infinity, the oscillators become less

coupled, as it approaches 1, then the oscillators are strongly coupled. Similarly, a_1/a_2 , large displacement/small displacement is defined as the coupling ratio for mode 8

By defining these ratios it is possible to see how the amount of coupling (i.e. how much one oscillator moves with respect to the other) between the oscillators for modes 7 and 8 changes with G-load.

4.2 Coupling vs. Geometry Study

If it is determined that mechanical coupling between the oscillators influences the frequency of the oscillators, it is necessary to see how changing the geometry can effect the coupling. Also, it is necessary to determine if changes in the geometry sacrifices scale factor (i.e. does it make the scale factor smaller, decreasing the resolution of the device?).

Using the beam Finite Element model described in Section 3, with its flexible proof mass, static and modal analysis were performed while varying the width of the force multiplier arm, the base beams and the flexures. Figure 4.4 illustrates the elements whose geometry changes in this analysis.

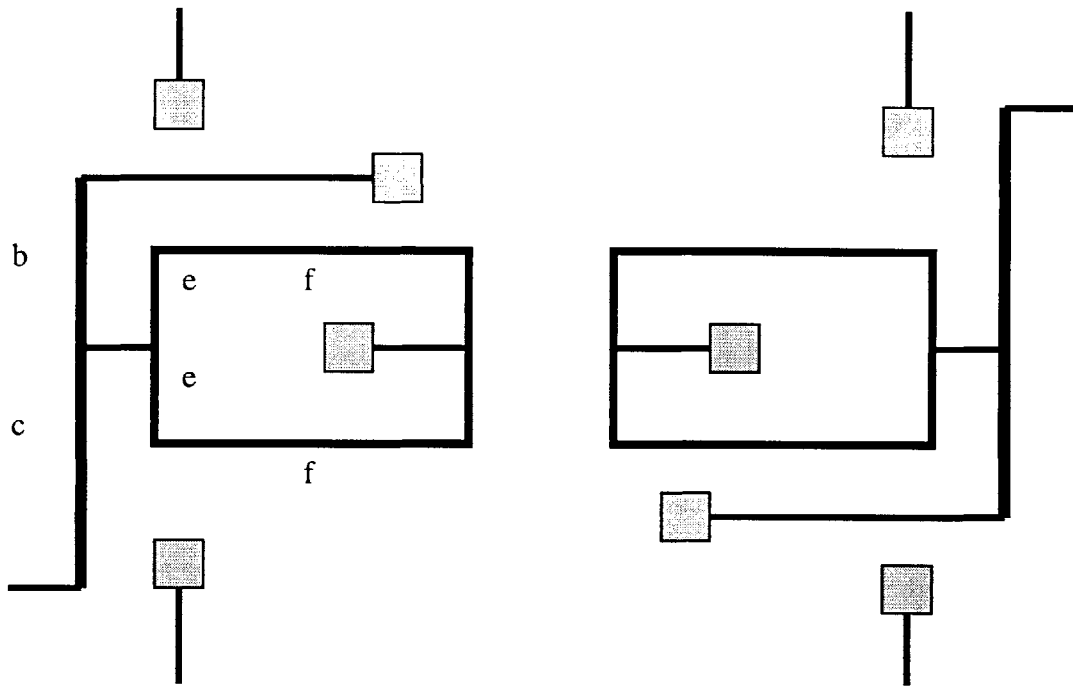


Figure 4.4 Beams whose widths are changes in iterations described in Table 5.1.

Twenty-three iterations were done, each time changing either the base beam width, the flexure width or the lever arm width. The flexures are much thinner than the base beams and the lever arm is much thicker than the base beams. Both of the base beams on an oscillator have the same thickness, as do both of the flexures.

4.2.1 Static Analysis

For each of the iterations of geometry changes, a static analysis was performed. Here, one of the oscillators is forced in the drive mode configuration while the other remains unforced. Figure 4.5 below shows the forces on the oscillator for the static analysis. The ratio (a_1/a_2 – see Figure 4.3) of the displacement of the forced oscillator to the resulting displacement of the passive oscillator is the zero-frequency coupling between the oscillators.

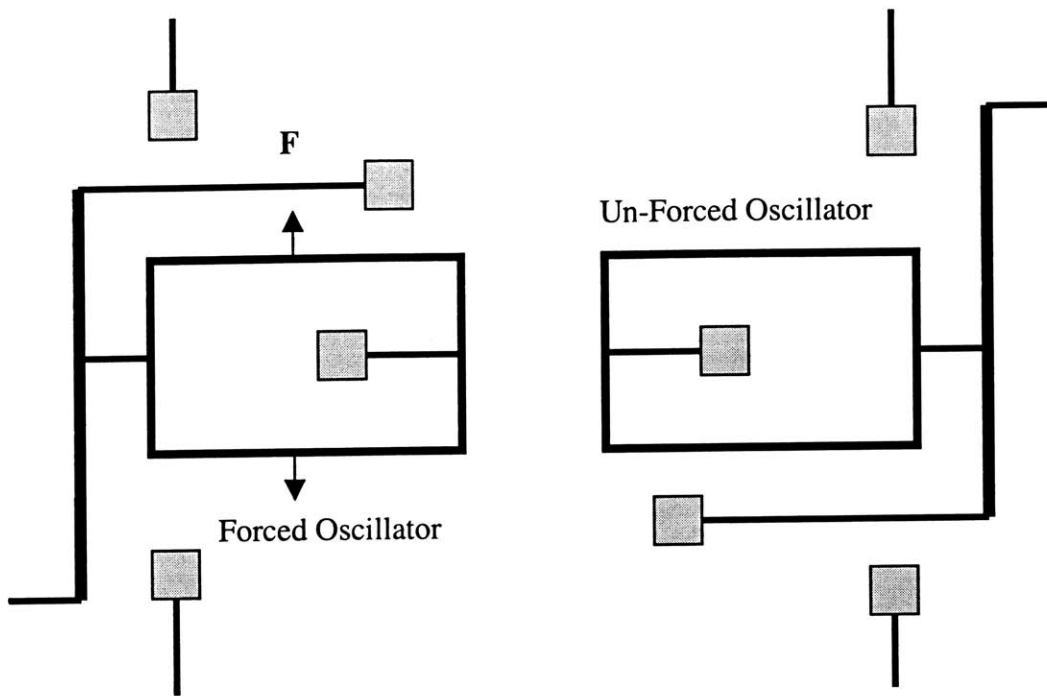


Figure 4.5 Forces on oscillator for static analysis.

4.2.2 Modal Analysis

For the same changes in dimensions, the frequency of the input axis mode was obtained to determine the effects of changing dimension on scale factor.

4.3 Mass Spring Model and Frequency Analysis

In this section a mass spring model of the SOA-3 is developed that will allow the effects of the coupling on the frequency difference between the oscillators to be obtained.

Figure 4.6 shows the mass spring model for the SOA-3. M_1 and k_1 represent the oscillator 1, and M_3 and k_3 represent the oscillator 2. M_2 represents the proof mass and is much larger than M_1 and M_3 . The stiffness of the proof mass and its support system are represented by k_2 . M_2 and k_2 couple the oscillators together. The coupling between the oscillators changes by varying the

value of k_2 . By increasing the value of k_2 , the spring becomes stiffer, decreasing the coupling between the oscillators. If the spring were completely rigid, the oscillators would be completely uncoupled; if k_2 is zero then the oscillators will have the maximum coupling.

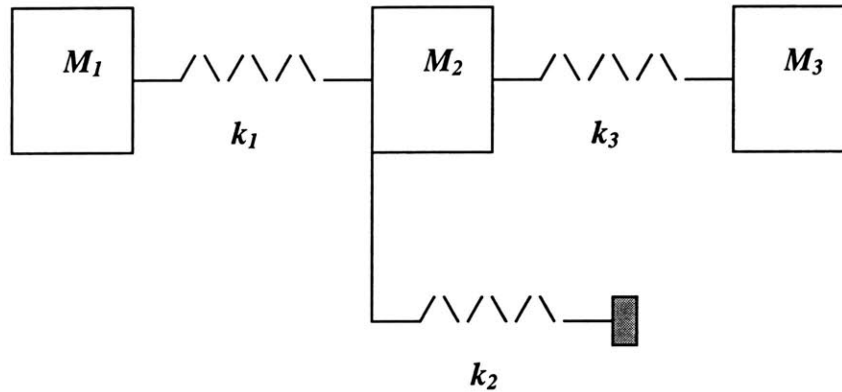


Figure 4.6 Mass spring model of the SOA-3.

The following are the equations of motion for the mass spring model of the system:

$$\begin{bmatrix} m_1 & 0 & 0 \\ 0 & m_2 & 0 \\ 0 & 0 & m_3 \end{bmatrix} \begin{Bmatrix} \ddot{x}_1 \\ \ddot{x}_2 \\ \ddot{x}_3 \end{Bmatrix} + \begin{bmatrix} k_1 & -k_1 & 0 \\ -k_1 & k_1 + k_2 + k_3 & -k_3 \\ 0 & -k_3 & k_3 \end{bmatrix} \begin{Bmatrix} x_1 \\ x_2 \\ x_3 \end{Bmatrix} = \begin{Bmatrix} 0 \\ 0 \\ 0 \end{Bmatrix}. \quad 4.3$$

The values for the masses are calculated from the solid model of the SOA. They remain the same even when the inertia load is changing. Because the model used here has identical oscillators, M_1 and M_3 have the same value. The values are:

$$m_1 = m_3 = 10^{-9} \text{ kg} \quad 4.4$$

$$m_2 = 2.25 * 10^{-9} \text{ kg} \quad 4.5$$

The stiffnesses when there is no external inertia load are:

$$k_1 = k_3 = 13 \frac{N}{m} \quad 4.6$$

$$k_2 = 1280 \frac{N}{m}. \quad 4.7$$

Again k_1 and k_3 are equal when the inertia load is zero because the oscillators are identical. The no-load stiffness of the proof mass is much greater than the stiffness of the oscillators.

Using modal analysis (see Appendix A), the eigenvalues and eigenvectors for the mass spring system are determined. The eigenvector reveals a mode that is mostly the movement of M_1 and another that is mostly the movement of M_3 . These correspond to the “drive modes” seen with the Finite Element model. As the external inertia load increases, the frequencies of the oscillators change. In this model, rather than putting a force on one of the masses in the model to change the oscillator frequencies, the frequency change in the oscillators is taken from the finite element model (see Figure 5.1 in Results section). The stiffness as a function inertia load can be found by taking the frequency of the oscillator at a specific inertia load and calculating the stiffness using the following relationship:

$$f = \frac{1}{2\pi} \sqrt{\frac{k}{m}} \quad 4.8$$

$$k = 2\pi f^2 m. \quad 4.9$$

The stiffness k_1 is taken from the frequencies associated with mode 7 (see in Appendix B) where oscillator 2 has very large amplitude and oscillator 1 has a very small amplitude. For the

sake of this model, it is assumed the frequency associated with mode 7 is solely the vibration of oscillator 1. So, oscillator 1 whose frequency increases with inertia load is the oscillator in tension. The stiffness k_3 is taken from frequencies associated with mode 8, which is primarily the motion of oscillator 2 and decreases with inertia load. Therefore oscillator 2 is in compression with a positive inertia load. Again, it is assumed that the frequency associated with mode 8 is solely the vibration on oscillator 2. Figure 5.1 in the results section shows the frequencies for mode 7 and mode 8 as a function of inertia load. Figure 5.9 in the results section then shows the stiffness for the oscillators as a function of inertia load.

In order to determine how the frequencies of vibration of the oscillators 1 and 2 change when they are coupled together by the proof mass, modal analysis is done on the system with four different values for the coupling spring, k_2 . Mathcad [4] was used to solve the modal analysis problems.

$k_2 = \text{infinity}$

First, a modal analysis of the system is done assuming that the coupling spring k_2 is infinitely stiff. This essentially decouples the oscillators and the frequency of one oscillator should have no effect on the frequency of the other. As noted above, k_1 and k_3 vary with G-load, with the values taken from the finite element model

$k_2 = \text{constant}$:

Second, modal analysis of the system will be done to obtain eigenvalues and eigenvectors holding k_2 constant at its no external inertia load value for the proof mass stiffness, 1280 N/m. This allows the proof mass to couple the two oscillators together. Again, k_1 and k_3 vary with inertia, with the values taken from the finite element model.

$k_2 = \text{zero}$

Third, the most coupling will occur between the two oscillators when the stiffness of the coupling spring is zero. Modal analysis is done to obtain the eigenvalues and eigenvectors for this value if k_2 . As before, k_1 and k_3 vary with inertia load and their values are taken from the finite element model.

$k_2 = (a_2/a_1) * 1280 \text{ N/m}$

Finally, if the results of the analysis done in Section 5.1.3 show that the coupling ratio (a_2/a_1) changes with the inertia load, then varying the stiffness of the coupling spring according to that ratio should reveal its significance. The ratio (a_2/a_1) is shown in Figure 5.3 in the Results section and $k_2 = (a_2/a_1) * 1280 \text{ N/m}$ along with k_1 and k_3 are shown in Figure 5.9.

For each of these scenarios, the system eigenvalues and eigenvectors are obtained. From the eigenvectors, the modes, which involve mostly M1 or mostly M3, are determined and their frequencies as a function of the applied inertia load can be plotted. Then, the readout of the system for each of the scenarios can be obtained using the following equations:

$$readout_{k_2=infinity} = f_{1k_2=infinity} - f_{3k_2=infinity} \quad 4.10$$

$$readout_{k_2=1280 \text{ N/m}} = f_{1k_2=1280 \text{ N/m}} - f_{3k_2=1280 \text{ N/m}} \quad 4.11$$

$$readout_{k_2=zero} = f_{1k_2=zero} - f_{3k_2=zero} \quad 4.12$$

$$readout_{k_2=(a_2/a_1)*1280} = f_{1k_2=(a_2/a_1)*1280} - f_{3k_2=(a_2/a_1)*1280} \quad 4.13$$

The frequency of oscillator 1 ($M1-k_1$) is represented by f_1 and the frequency of oscillator 2 ($M3-k_3$) is represented by f_2 . The error in the device readout due to the coupling by the proof mass is the difference in the readout for $k_2=1280N/m$ and the readout for $k_2=\text{infinity}$. represented by equation 4.12:

$$error_{1280-\text{infinity}} = readout_{k_2=1280N/m} - readout_{k_2=\text{infinity}} \cdot \quad 4.14$$

$$error_{\text{zero}-\text{infinity}} = readout_{k_2=\text{zero}} - readout_{k_2=\text{infinity}} \quad 4.15$$

$$error_{(\frac{a_2}{a_1}) * 1280 - \text{infinity}} = readout_{k_2=(\frac{a_2}{a_1}) * 1280N/m} - readout_{k_2=\text{infinity}} \cdot \quad 4.16$$

5 Results

5.1 Defining Coupling

There are several important results that arose from the analysis done to define coupling. The degree of coupling between the oscillators is a function of the inertia load applied to the accelerometer; the uncoupled frequency curves intersect at zero inertia load; the coupled frequency curves converge at zero inertia load but do not intersect. These results are discussed in detail in the following sections.

5.1.1 Frequencies for Modes 7 and 8

First it must be confirmed that the cross-over frequency (the point at which the frequencies of the two oscillators converge or intersect) is in fact at zero input acceleration; which corresponds to zero inertia load. Figure 5.1 shows the frequencies for modes 7 and 8. From Figure 5.1 it appears that their frequencies do cross at zero. The frequency for mode 7 decreases linearly with increased inertia load because mode 7 is primarily the motion of the oscillator in compression. The frequency for mode 8 increases linearly with inertia load because it is primarily the motion of the oscillator in tension. When the frequencies of the oscillators are

measured during the operation of the device they will exhibit the same frequency behavior as modes 7 and 8.

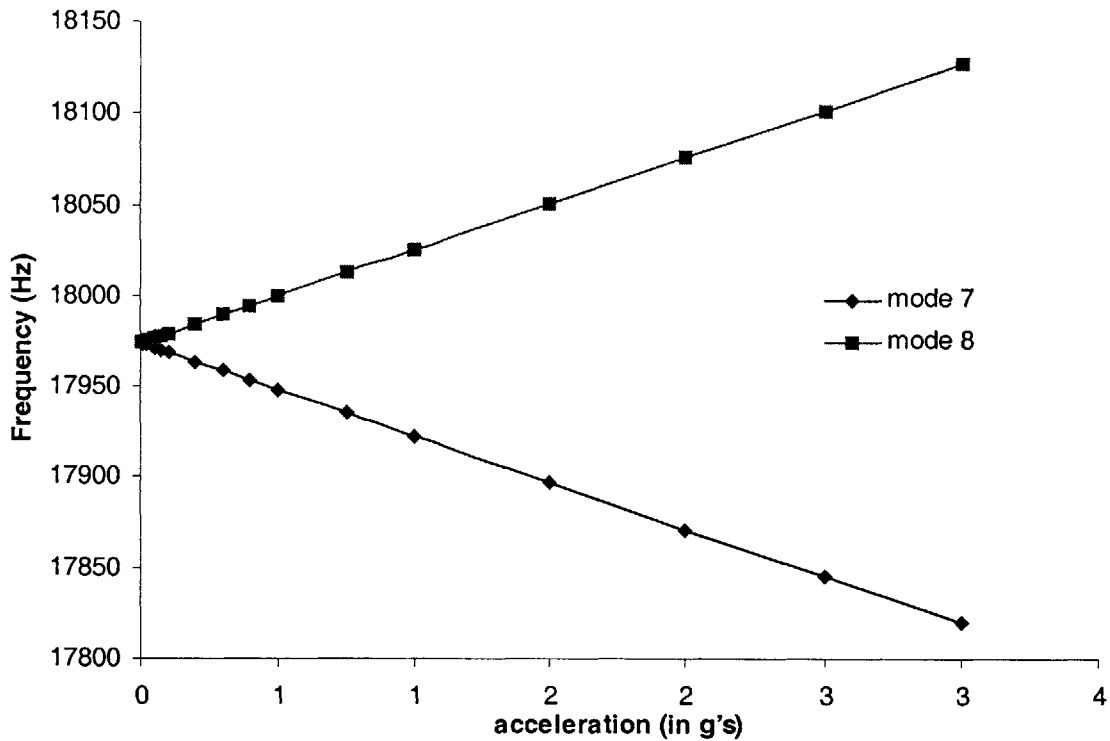


Figure 5.1 Frequencies of modes 7 and 8 as a function of input acceleration.

Figure 5.2 shows the frequencies of modes 7 and 8 from 0 to 500 μg . This figure shows that the frequencies of modes 7 and 8 never intersect. Mode 7 levels off at 17974.12 Hz and mode 8 at 17974.14 Hz starting at 0 continuing to 100 μg . The arrows in the figure show the frequency paths for each oscillator. When the inertia load is negative, the frequency of oscillator 1 follows mode 7. At 0 g, which would be the frequency intersection point in the uncoupled case, the frequency becomes mode 8 causing a discontinuity in the frequency readout for the oscillator. The opposite is true for oscillator 2. The discontinuity produces an error of 0.2 Hz at the frequency crossover point.

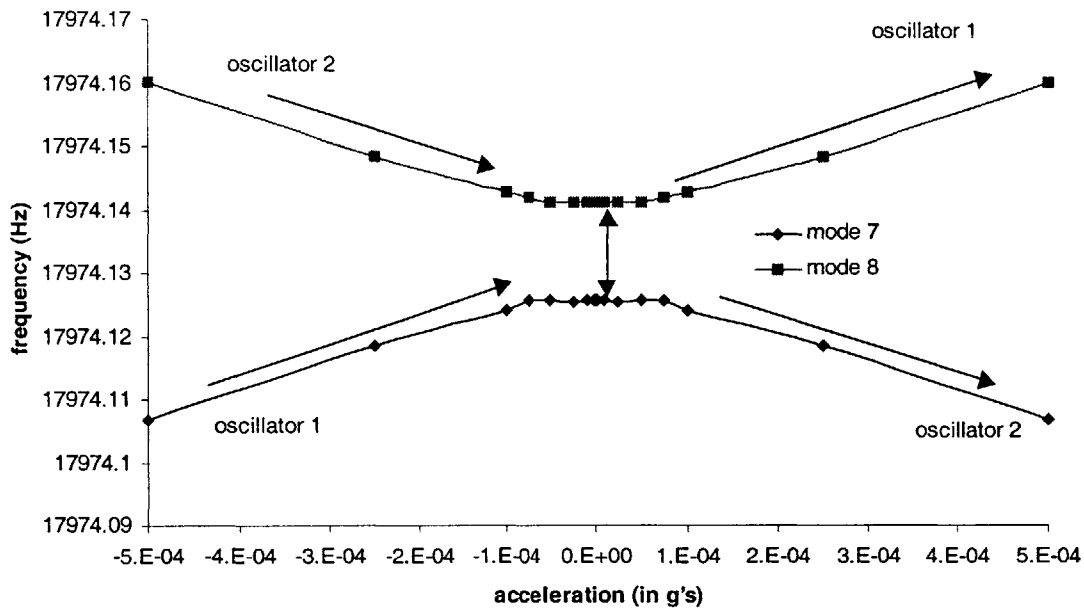


Figure 5.2 Frequencies for modes 7 and 8 as a function of input acceleration near the frequency crossover point

5.1.2 Coupling Ratio

Figure 5.3 below shows the coupling ratios, which is the large oscillator displacement divided by the small oscillator displacement for both modes 7 and 8. These coupling ratios, a_1/a_2 and a_2/a_1 were defined in section 4.1.3. From the plot of coupling ratio versus acceleration applied to the device, it is seen that the coupling ratios do change when the acceleration changes. For each acceleration there is a specific amount that one oscillator will be displaced with respect to the other in each of the drive modes 7 and 8.

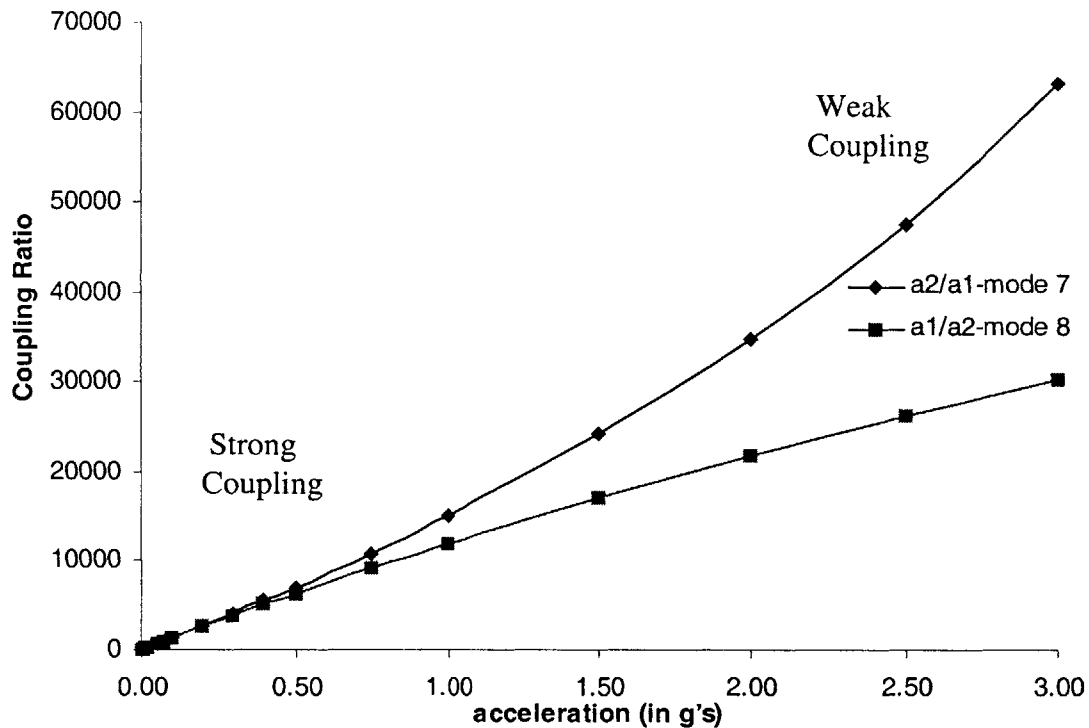


Figure 5.3 Coupling ratio for modes 7 and 8 as a function of acceleration.

This plot shows that the general trend for the coupling ratio a_1/a_2 over a large range of acceleration is linear for mode 8, which is mostly the movement of the oscillator in tension and a_2/a_1 is almost linear for mode 7, which is mostly the movement of the oscillator in compression. Because the oscillators are equal and the frequency for modes 7 and 8 change at equal and opposite rates, the fact that their coupling ratios are not identical is unexpected. This may indicate that equal tensile and compressive loads on each of the oscillators do not have an equal effect on their coupling. Also, because the coupling ratio decreases as the frequency cross-over point is approached, it means that the difference between a_1 and a_2 is decreasing. This means that either a_2 is increasing or a_1 decreasing or both meaning that the two oscillators are more coupled together. Thus, because the coupling between the two oscillators increases, the coupling ratio decreases as the input acceleration approaches zero.

After observing the general trend for the coupling ratio it is important to also take a look at the behavior of this ratio near the frequency crossover point. Figure 5.4 shows the coupling ratio from 0 to 500 μg 's for modes 7 and 8. In this range the coupling ratio again appears to increase nearly linearly with the inertia load except in the range from 0 to 0.1 μg . Also, in the range from 0 to 500 μg the coupling ratios for modes 7 and 8 are the same. So, in general in the 0 to 500 μg range, the coupling again increases as the acceleration approaches zero and is the strongest at the crossover frequency.

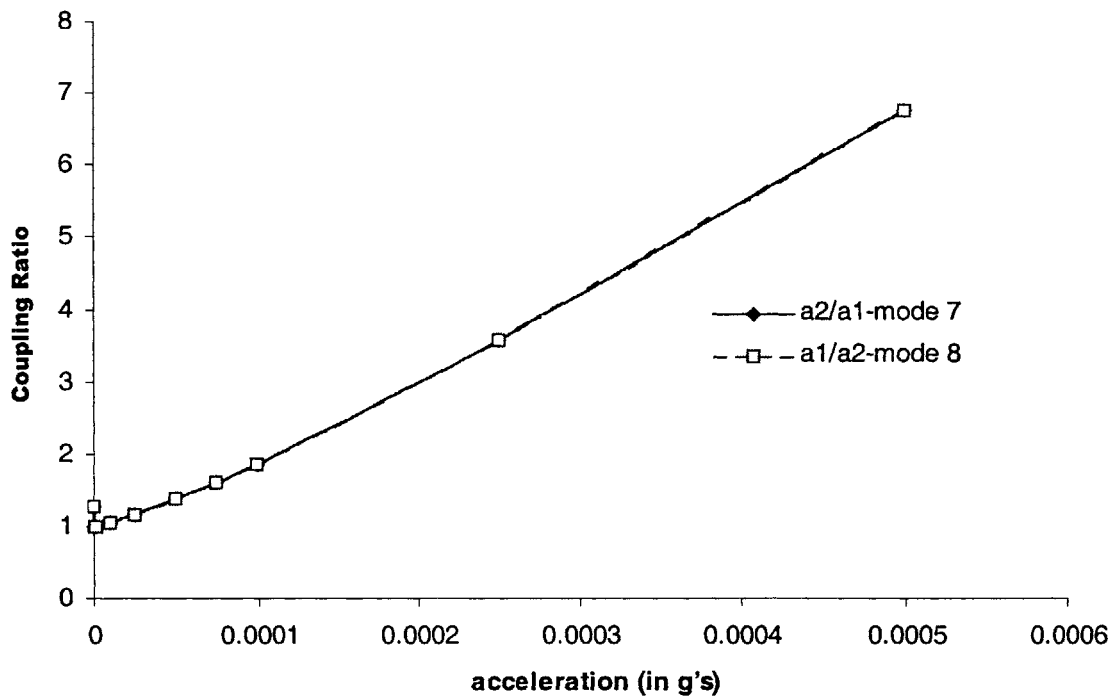


Figure 5.4 Coupling ratio for modes 7 and 8 as a function of inertia load near the frequency crossover point.

It is difficult to see the section from 0 to 0.1 μg in Figure 5.4 so Figure 5.5 shows the coupling ratio from 0 to 0.1 μg . This figure shows that in the 0 to 0.1 μg range the coupling ratio for both modes oscillates slightly around a constant value of 1. At this point, the tensile and

compressive loads on the oscillators are almost zero and have little effect on displacement of the oscillators. And again, the coupling ratio is almost the same for both modes.

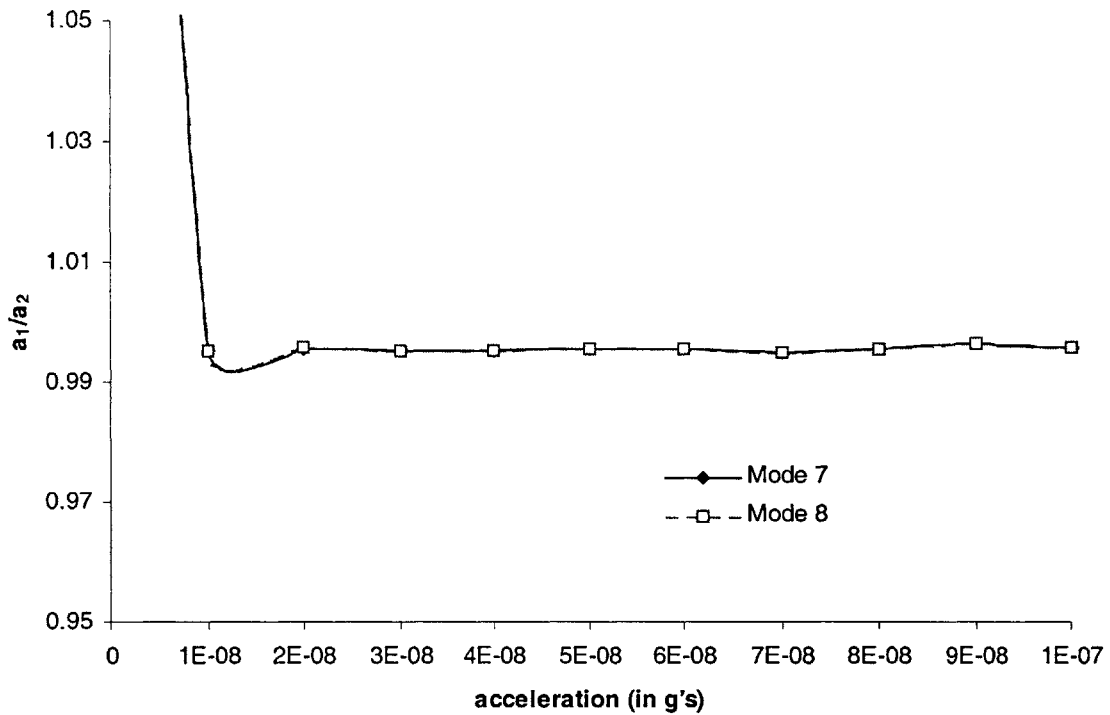


Figure 5.5 Coupling ratios for modes 7 and 8 for the range of 0 to .1 microg.

5.2 Coupling vs. Geometry Study

The following results arose from changing the widths of several elements in the SOA-3. In this section the effects of changing the geometry on the coupling between the oscillators and on the scale factor are outlined.

5.2.1 Base Beam Width:

Figure 5.6 below shows the effects of changing the base beam width on the coupling, defined in section 4.3 to be a_1/a_2 in Figure 4.5 and the input axis mode frequency of the device.

the original normalized base beam width is 1. The input axis frequencies are normalized to this value.

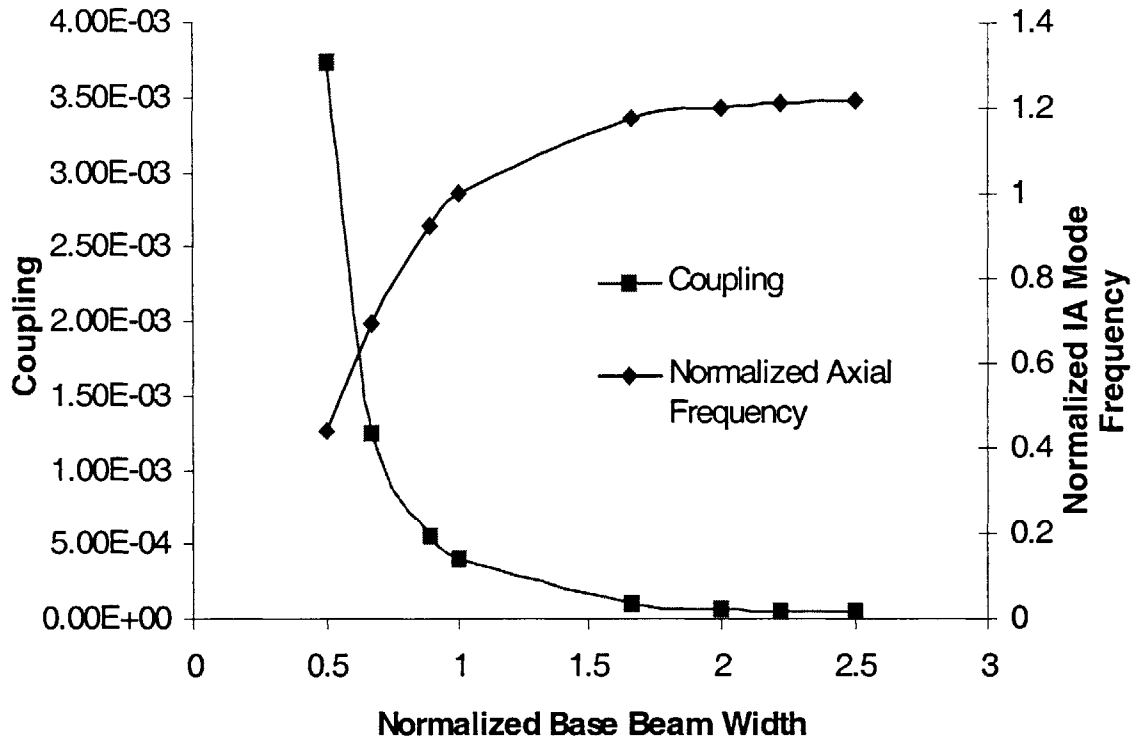


Figure 5.6 Coupling and input axis mode frequency as a function of base beam width.

As shown in the plot, doubling the normalized width from 1 to 2 decreases the coupling. Increasing the width of the base beams makes them more rigid, causing them to put the flexures in tension or compression rather than making them buckle. Therefore, doubling the width has little effect on scale factor because it causes the normalized input axis frequency to increase by 25%. Increasing the beam width to more than double its original value has only slightly more effect because the decrease in coupling and increase in normalized input axis frequency seem to level off.

5.2.2 Flexure Width

Similarly, the effects of changing the flexure widths on the coupling and input axis frequency are shown in Figure 5.7. The original normalized flexure width is 1. The input axis mode frequency is normalized to its value at this width. Increasing the width causes the coupling and the input axis mode frequency to increase. In a thesis done by Nathan St.Michel at Draper Laboratory a correlation is made between increased input axis mode frequency due to changes in flexure width and increased scale factor.[9] Using that correlation it is inferred that the increase in input axis frequency sacrifices the scale factor of the device. But, cutting the width in half, decreases the coupling by half and the normalized input axis frequency decreases slightly.

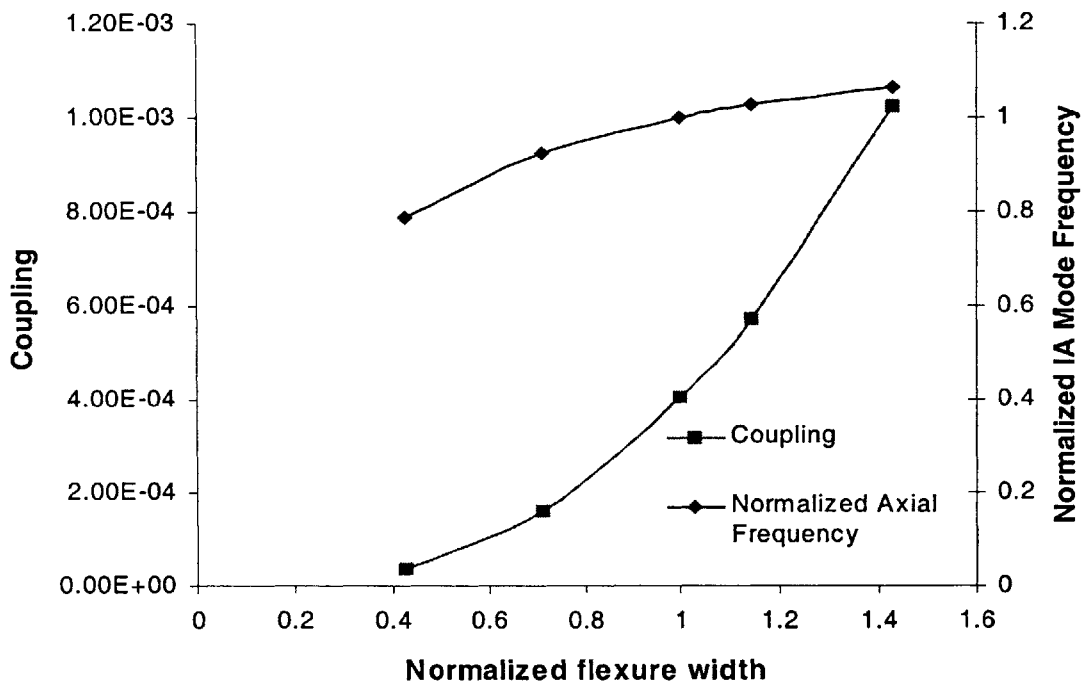


Figure 5.7 Coupling and input axis mode frequency as a function of flexure width.

5.2.3 Lever Arm Width

Finally, changing the width of the lever arm also had some effect on the coupling and the input axis frequency as shown in Figure 5.8 below. The original normalized lever arm width is 1 and the input axis mode frequency is normalized to its value at this width. Increasing the lever arm width had little effect on the coupling yet increased the frequency of the input axis mode. However, decreasing the lever arm width from 1 to 1/3, making it less rigid, dropped the coupling to half its original value and also decreased the input axis mode frequency.

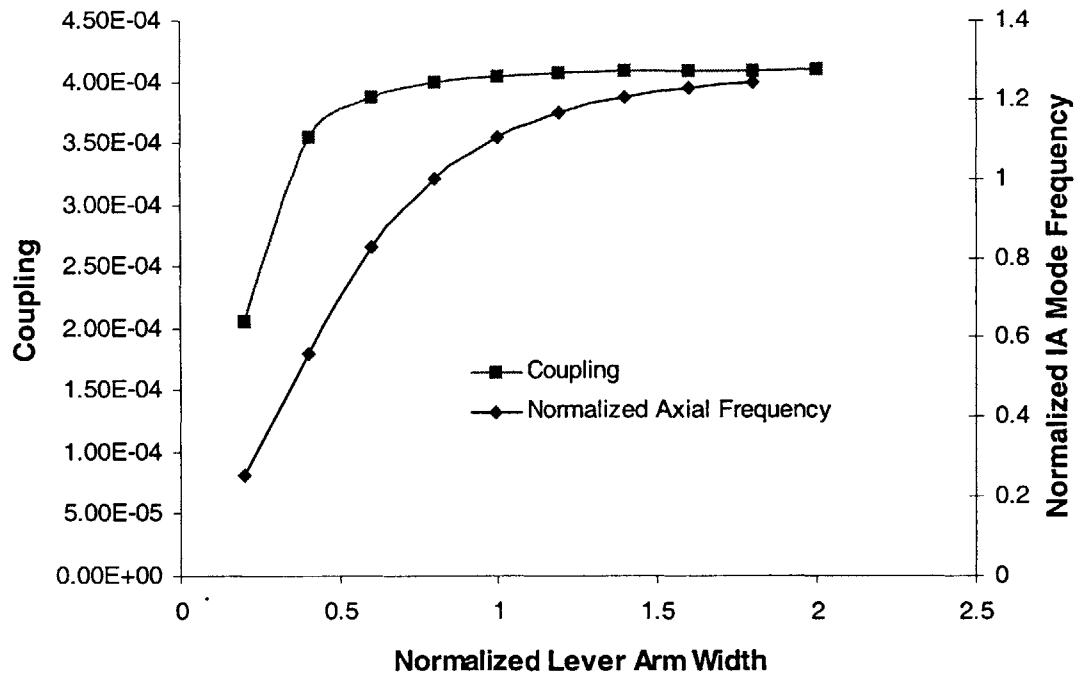


Figure 5.8 Coupling and input axis mode frequency as a function of lever arm width.

5.3 Mass Spring Model and Frequency Analysis

Using these frequencies shown in Figure 5.1 and the coupling ratios shown in Figure 5.3, the stiffnesses for the springs in Section 4.3's mass spring model can be determined with equation 4.9. They are plotted in Figure 5.9 below.

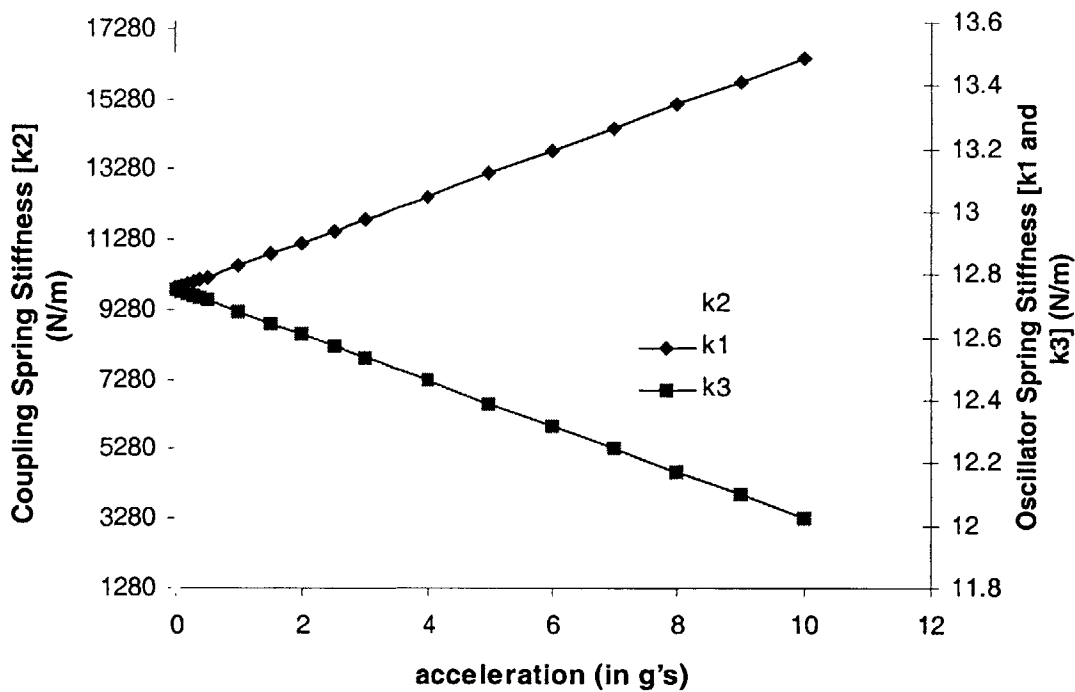


Figure 5.9 Stiffnesses for oscillator and coupling springs in Section 5.3's mass spring model.

The results in this section were obtained using the mass spring model developed in section 4.4. The mass spring model gave some conclusive results about the effects of coupling on the frequencies of the oscillators and thus the readout of the device. Figure 6.10 below shows the frequencies of oscillators M1-k1 and M3-k3 in the model for each of the values assigned to k2 in section 5.4, from 0 g to 10 g. The frequencies of oscillators M1-k1 and M3-k3 when $k_2=1280\text{N/m}$ are represented by "M1 k2=1280" and "M3 k2=1280" respectively. The frequencies for oscillators M1-k1 and M3-k3 when $k_2=\text{infinity}$ are represented by "M1 k2=infinity" and "M3 k2= infinity" respectively. The frequencies for oscillators M1-k1 and M3-k3 when $k_2=\text{zero}$ are represented by "M1 k2=zero" and "M3 k2= zero" respectively. Finally, the

frequencies for oscillators M1-k1 and M3-k3 when $k_2=(a_2/a_1)*1280 \text{ N/m}$ are represented by “M1 $k_2=(a_2/a_1)*1280$ ” and “M3 $k_2=(a_2/a_1)*1280$ ” respectively.

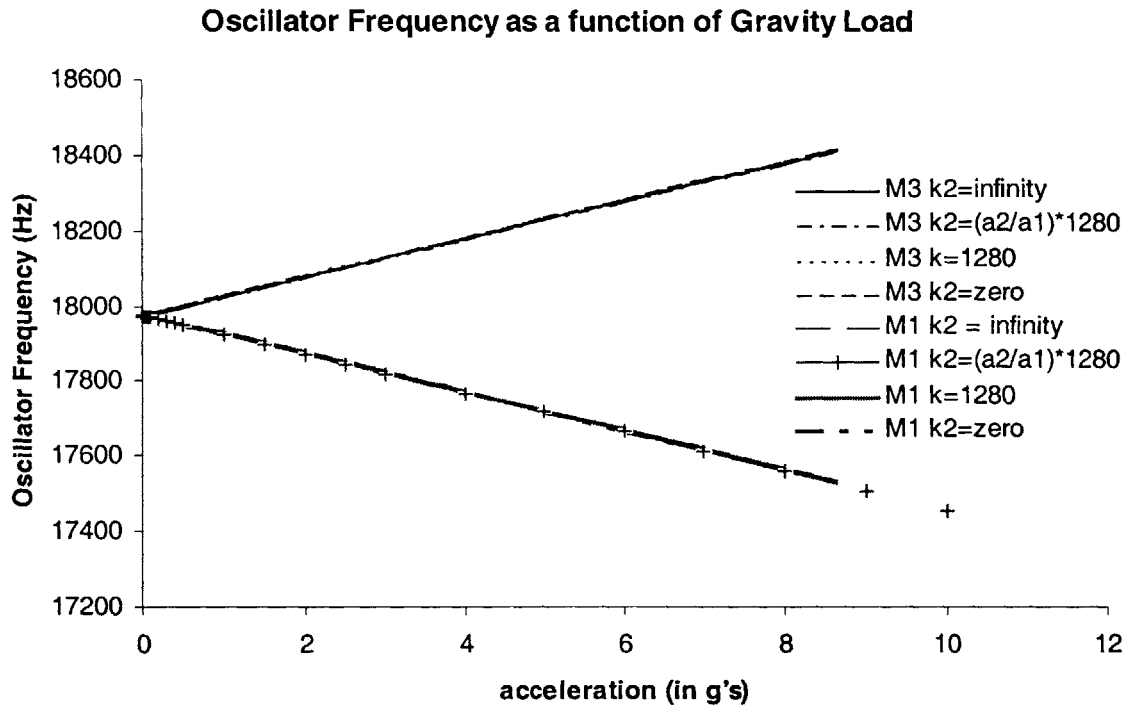


Figure 5.10 Oscillator frequency as a function of inertia load.

In the figure the frequencies for each of the oscillators in each of the cases appear to be linear over the broad range of acceleration. Figure 5.11 shows the same information as Figure 5.10 but only for acceleration from 0 g to .25 g, which is near the frequency crossover point.

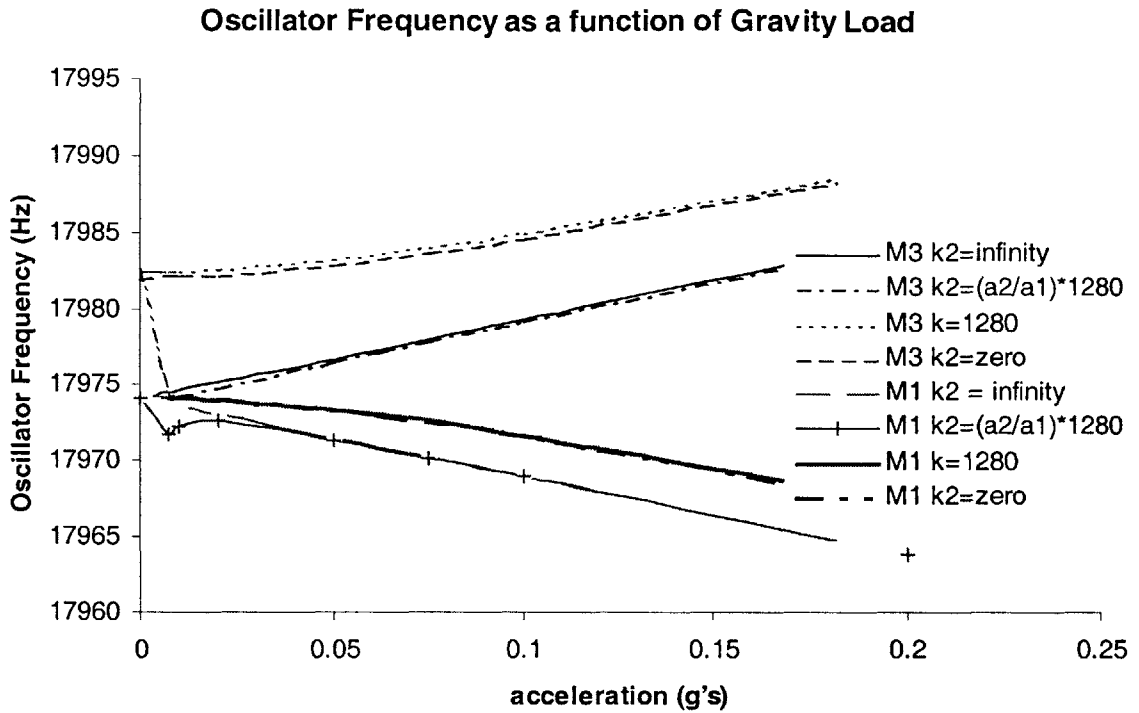


Figure 5.11 Oscillator frequency as a function of acceleration near frequency crossover point.

Figure 5.11 shows that when k_2 is 1280 N/m , zero and $(a_2/a_1)*1280 N/m$ the frequencies of the oscillators do not intersect. This is similar to the information seen in Figure 5.2, which represents the frequencies of the oscillators in the SOA-3 taken from the Finite Element model. When k_2 is infinite, the frequencies of the two oscillators do intersect because they are completely uncoupled. With increased acceleration, there is an increase in detuning (or separating of the frequencies) of the oscillators in each of the cases. The frequency offsets due to coupling (i.e. in every case but when k_2 is infinite) are greatest near zero and decrease as the acceleration increases. The frequency offset due to the coupling was the greatest in the $k_2 = 1280 N/m$ case. The offset was slightly less in when the coupling stiffness was zero and in the case where $k_2=(a_2/a_1)*1280 N/m$ the offset was large near zero inertia load but quickly decreased. Changing the value of (a_2/a_1) would change the rate at which the offset decreased. The

unexpected result was that the offset for the zero stiffness case was not the greatest. With the oscillators in the most coupled situation, the offset should have been the greatest in this case.

The readouts for the device for each of the cases, defined by Equations 4.10 through 4.13, are shown in Figure 5.12 and 5.13 below. The device readout for each of the cases appears to increase linearly over the range from 0 g to 10 g but in the range from 0 to 0.25 g there is an offset in the readout for the cases of $k_2=1280\text{ N/m}$, $k_2=(a_2/a_1)*1280\text{ N/m}$ and $k_2=\text{zero}$.

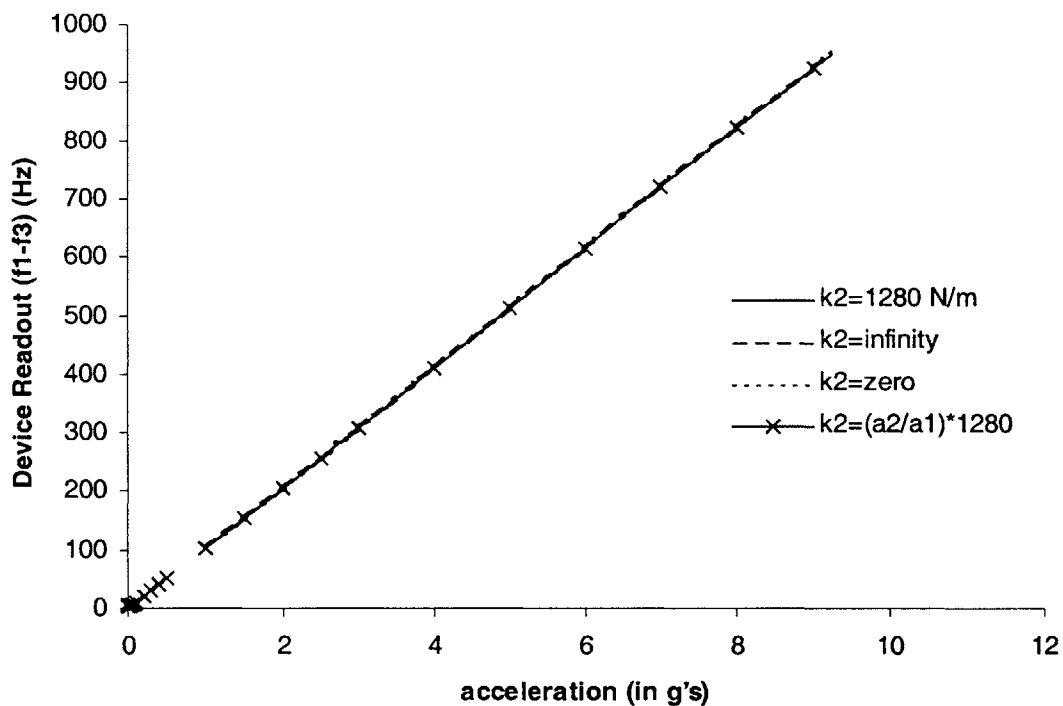


Figure 5.12 Device readout as a function of acceleration.

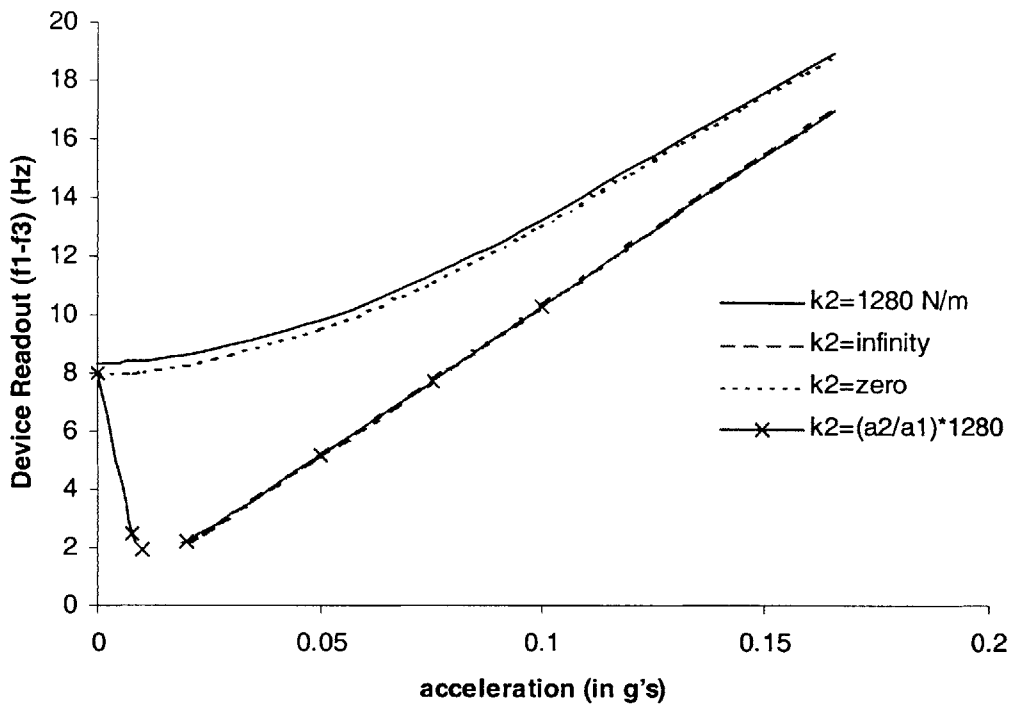


Figure 5.13 Device readout as a function of acceleration near the frequency cross-over point.

It is difficult to see the difference between the curves in Figures 5.12 and 5.13, so the difference or “error” is plotted in Figure 5.14 below. The error shown in this plot is the error due to the coupling of the two oscillators by the proof mass. As seen in the plot, the error is greatest near the frequency crossover point, which agrees with the information given in Figure 5.3, which says that the coupling is the greatest near the frequency crossover point. The error continues to decrease until about acceleration. So the real error due to coupling is the error shown on the plot at a certain acceleration minus this constant value. So, after a certain inertia load, the oscillators act like uncoupled oscillators and the error due to coupling is essentially zero.

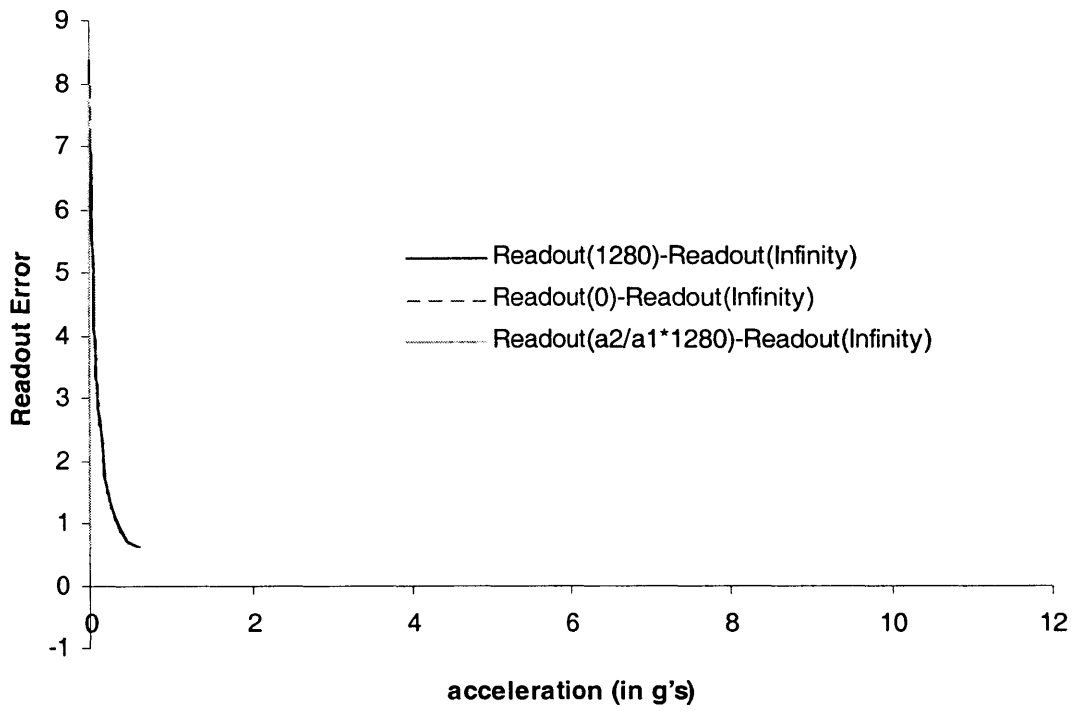


Figure 5.14 Frequency readout error as a function of acceleration.

6 Recommendations and Conclusions:

This study proves that there is mechanical coupling between the oscillators in Draper Laboratory's third generation micromechanical Silicon Oscillating Accelerometer. By measuring the ratios of the displacement of one oscillator to the other in each of the system's drive modes, a "coupling ratio" was established as a function of the inertia load applied to the device. This coupling ratio showed that the coupling between the oscillators is strongest near the frequency cross-over point and decreases with increased inertia load. This is true for both of the drive modes.

Changing the geometry of the device also affects the mechanical coupling. Increasing the base beam width decreases the coupling between the oscillators the most, while decreasing the flexure width also decreases the coupling. However, increasing the widths of the base beams and the flexures increases the frequency of vibration of the proof mass along the input axis, which causes the scale factor for the device to increase. Also, decreasing the width of the lever arm decreased the coupling slightly and decreased the frequency of vibration for the proof mass. These geometry changes would decrease the amount of coupling between the oscillators, but it must be considered how these changes will affect other aspects of the device's design and operation.

The effects of coupling on the frequencies of the oscillators were determined by postulating a simple chain-like spring-mass model of the Silicon Oscillating Accelerometer, see Figure 4.6. The degree of coupling between the oscillators was modeled by varying the stiffness of the central spring, which ties the model to the substrate. When the value of this spring stiffness is infinite, the oscillators are uncoupled and the two frequency branches vary linearly with input acceleration, see Figure 5.10; the difference between these two branches (frequency readout) also varies linearly with the input acceleration, see Figure 5.12. The effect of coupling was assessed in two ways: first by assigning a constant value of stiffness to the coupling spring; and second by assuming a stiffness that varied in proportion to the coupling ratio a_2/a_1 . In the first case, the readout error was greatest near the uncoupled frequency crossover point and quickly decreased to a finite value as the input acceleration increased, see Figure 5.14. In the second case, the readout error was again largest at the frequency crossover point but in this case rapidly decreased to zero, again see Figure 5.14. It may be inferred that the rate of decrease of the readout error is a function of the degree of mechanical coupling between the oscillators.

Using the Finite Element model, described in section 3.7, which represents a coupled system, the frequencies of the oscillators were obtained. This confirmed the validity of the way the coupling was modeled in the mass-spring model and also showed that there is a discontinuity in the frequency readout at the frequency crossover point. It is believed that this discontinuity causes an error in frequency readout of at least 0.2 Hz at that point. This error due to the discontinuity could be larger than 0.2 Hz, depending on how the oscillator is tied to the proof mass in the shell element model. Because there are several ways of doing this, it is suggested that further study be done on this using a full solid Finite Element model rather than shell elements.

In general, the mechanical coupling does effect the readout of the instrument, especially in the vicinity of the frequency crossover point. The exact physical mechanism of this mechanical coupling has yet to be identified and further work to establish this mechanism is recommended.

Appendix A: Overview of Modal Analysis

[7]

For more information on this subject see *Fundamentals of Applied Dynamics* by Williams. [11]

Eigenvalue Problem:

$$[A]\{x\} = \lambda\{x\} \quad \text{A.1}$$

- $[A]$ is real and invertible
- $\lambda_1, \lambda_2, \dots$ are called eigenvalues.
- $\{g_1\}, \{g_2\}, \dots$ are the eigenvectors associated with the eigenvalues.

1.) The eigenvectors are orthogonal

$$\text{Error! Not a valid embedded object., } i \neq j. \quad \text{A.2}$$

2.) If $[A]$ is transformed into the orthogonal coordinate system given by the eigenvectors, $[A]$ becomes diagonal with the eigenvalues on the diagonal.

Eigenvalue Analysis applied to Equations of Motion for a System:

Equation of Motion for System:

Error! Not a valid embedded object..

A.3

\mathbf{M} is the mass matrix and \mathbf{K} is the stiffness matrix associated with the system. \mathbf{K} and \mathbf{M} are symmetric and \mathbf{M} is positive definite. Assume that this differential equation has solutions of the form:

$$\{x\} = \{c\}e^{i\omega t}. \quad \text{A.4}$$

Substituting Equation A1.4 into Equation A1.3,

$$-\omega^2 [\mathbf{M}]\{c\} + [\mathbf{K}]\{c\} = 0 \quad \text{A.5}$$

$$[\mathbf{K}]\{c\} = \omega^2 [\mathbf{M}]\{c\}. \quad \text{A.6}$$

- $\omega_1^2, \omega_2^2 \dots \omega_n^2$ are the eigenvalues and ω_i are the natural frequencies of the system.
- $\{\varphi\}_1, \{\varphi\}_2, \dots, \{\varphi\}_n$ are their associated eigenvalues which are the natural mode shapes of the system.
- The eigenvalues are real and positive.
- Weighted, simultaneous orthogonality:

$$\{\varphi_i\}^T [\mathbf{M}]\{\varphi_j\} = 0 \quad i \neq j \quad \text{A.7}$$

$$\{\varphi_i\}^T [\mathbf{K}]\{\varphi_j\} = 0 \quad i = j. \quad \text{A.8}$$

The Modal Matrix is then

$$[\Phi] = \{ \{\varphi_1\}, \{\varphi_2\}, \dots \}. \quad \text{A.9}$$

The modal masses are a diagonal matrix with m_i terms on the diagonal.

$$[\Phi]^T [M] [\Phi] = \begin{bmatrix} m_{11} & 0 & 0 \\ 0 & . & 0 \\ 0 & 0 & m_{ii} \end{bmatrix} \quad \text{A.10}$$

The modal stiffnesses are a diagonal matrix with k_i terms on the diagonal.

$$[\Phi]^T [K] [\Phi] = \begin{bmatrix} k_{11} & 0 & 0 \\ 0 & . & 0 \\ 0 & 0 & k_{ii} \end{bmatrix} \quad \text{A.11}$$

Mass normalizing the eigenvectors:

$$\{\Psi_i\} = \frac{1}{\sqrt{m_i}} \{\varphi_i\} \quad \text{A.12}$$

Then Ψ is the modal matrix and the following relationships are true:

$$[\Psi]^T [M] [\Psi] = [I] \quad \text{A.13}$$

$$[\Psi]^T [K] [\Psi] = \begin{bmatrix} \omega^2_{11} & 0 & 0 \\ 0 & . & 0 \\ 0 & 0 & \omega^2_{ii} \end{bmatrix} = \text{spectral matrix.} \quad \text{A.14}$$

Method of Modal Superposition:

Equation of motion for the system with a force $f(t)$:

$$[M]_{N \times N} \left\{ \ddot{x} \right\} + [K] \{x\} = f(t). \quad \text{A.15}$$

This problem can be broken down into two smaller problems:

Part 1: Eigenvalue Problem

- Set $\{f(t)\} = 0$ (i.e. free vibration) so Equations A1.4 and A1.6 from above are true.
- Find the mass normalized modal matrix, and the spectral matrix.

Part 2: Vibration Problem:

Step 1: introduce a modal coordinate $\{q\}$ such that

$$\{x\} = [\Psi] \{q\}. \quad \text{A.16}$$

Now the equations of motion for the system become,

$$[M] [\Psi] \left\{ \ddot{q} \right\} + [K] [\Psi] \{q\} = f(t). \quad \text{A.17}$$

Premultiplying by $[\Psi]^T$ results in N uncoupled equations, each a single degree of freedom system.

$$[I]\{\ddot{q}\} + \begin{bmatrix} \omega^2_{11} & 0 & 0 \\ 0 & . & 0 \\ 0 & 0 & \omega^2_{ii} \end{bmatrix} \{q\} = [\Psi]^T \{f(t)\}. \quad \text{A.18}$$

State Space Equations

Equation A.18 can be translated to a state-space equation of motion using the following relationships:

$$A_{n \times n} = \begin{bmatrix} 0 & I \\ [-\omega_n^2] & 0 \end{bmatrix} \quad \text{A.19}$$

$$B_{n \times n} = [[\Psi][f(t)]] \quad \text{A.20}$$

where u is the system inputs.

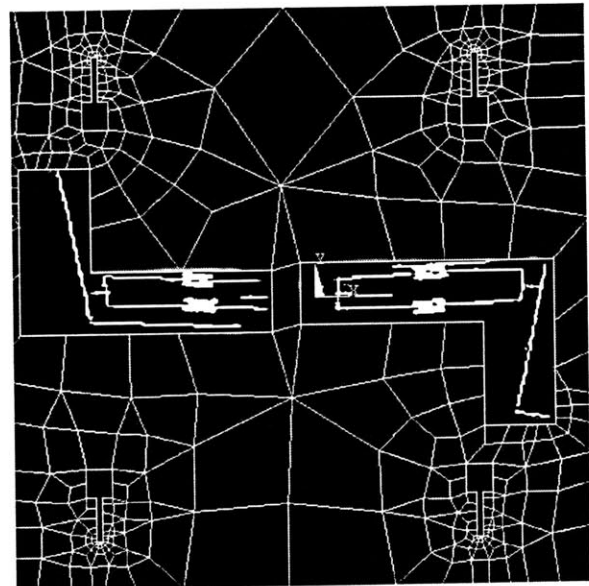
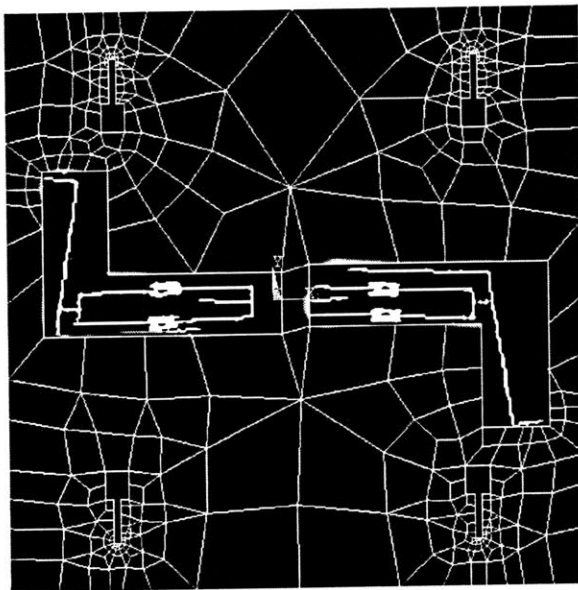
The equation of motion for the system is then:

$$\begin{Bmatrix} \dot{x} \\ x \end{Bmatrix} = A_{n \times n} \{x\} + B_{n \times u} \{u\}. \quad \text{A.21}$$

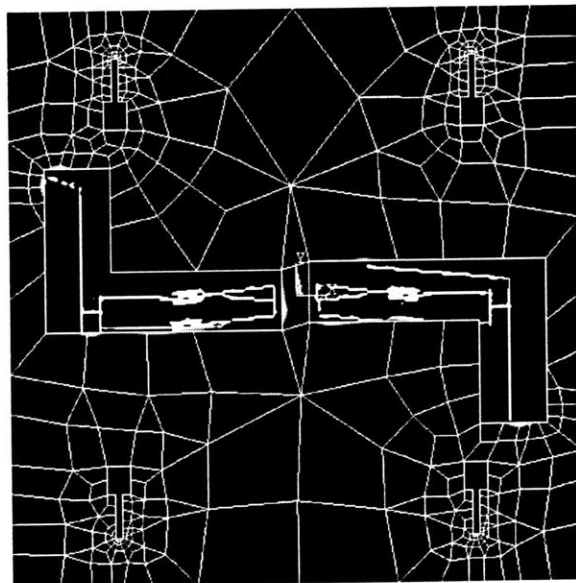
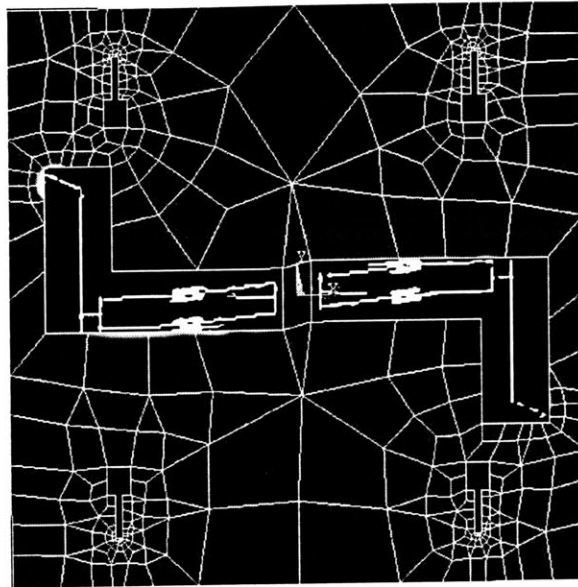
Appendix B: Mode Shapes of the SOA-3

The mode shapes for the system are shown below in order of increasing frequency:

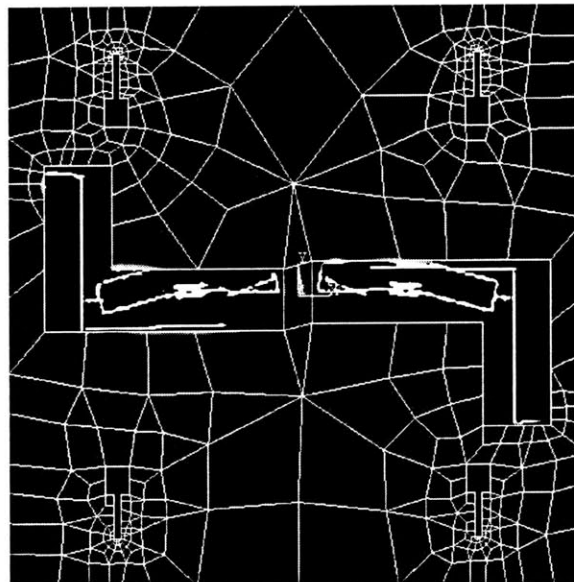
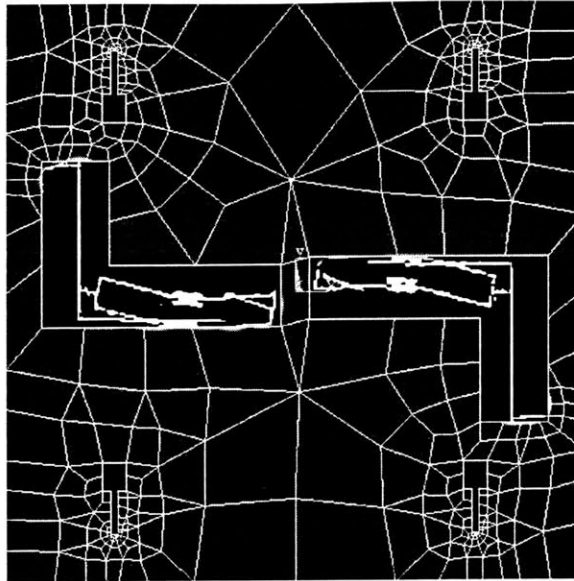
Mode 1: Input Axis Mode



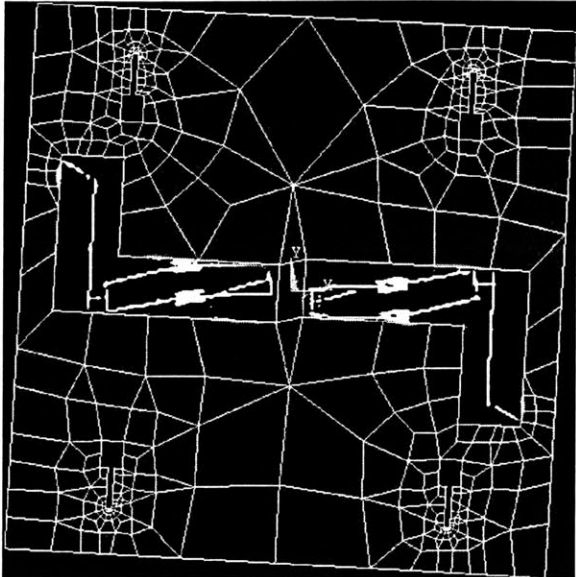
Modes 2 and 3: Proof mass Bending Modes



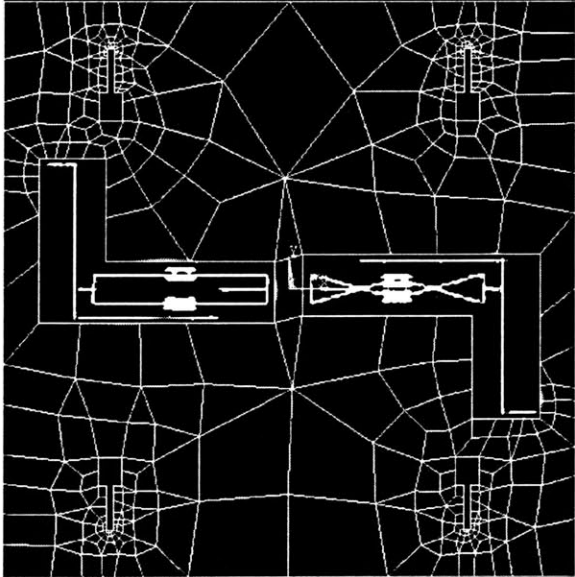
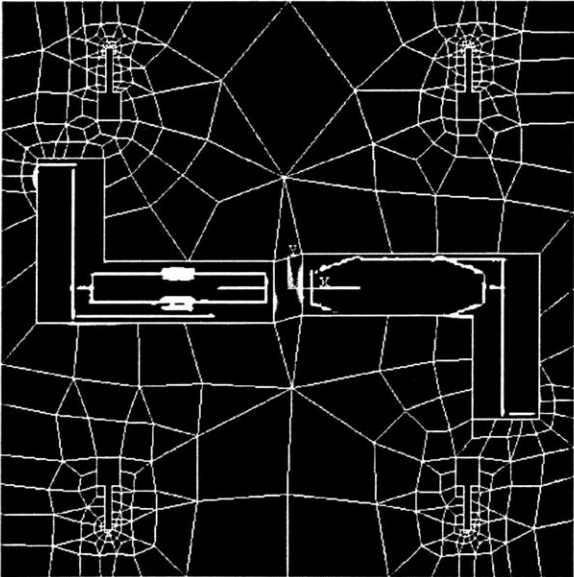
Modes 4 and 5: Hula Modes

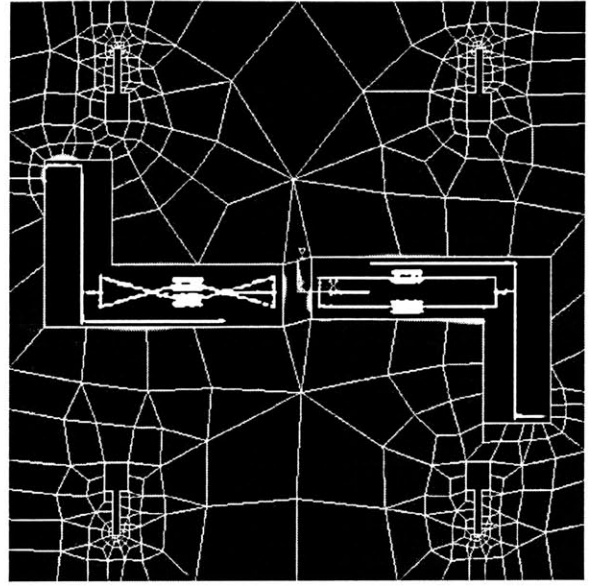
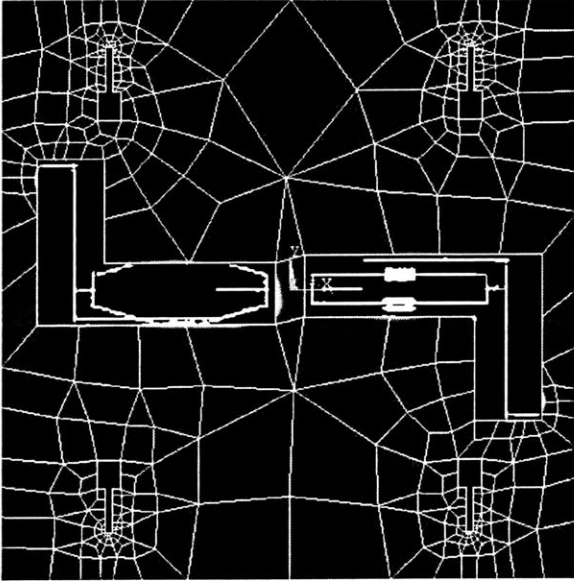


Mode 6: Proof mass Twisting Mode



Modes 7 and 8: Drive Modes





Bibliography

- [1] Ansys, version 5.6.2 copyright 1994, Ansys, Inc.
- [2] Chandrupatla, T.R., Belegundu, A.D., *Introduction to Finite Elements in Engineering*. Chapter 11. Prentice-Hall, Inc., 1997.
- [3] Hopkins, R., Borenstein, J., Antkowiak, B., Ward, P., Elliot, R., Weinberg, M., DePiero, M., Miola, J., “The Silicon Oscillating Accelerometer: A MEMS Inertial Instrument for Strategic Missile Guidance,” AIAA Missile Sciences Conference, Paper CSDL-P-3801, Oct 2000.
- [4] Mathcad 2000 Professional, copyright 1999, Mathsoft, Inc.
- [5] Nastran, version 70.5.5, copyright 1999, MacNeal-Schwendler Corporation.
- [6] One-dimensional model created for this project by Bernie Antkowiak of Draper Laboratory.
- [7] Overview created for this project by Dr. Frederick Nelson of Draper Laboratory.
- [8] ProEngineer, copyright 1998, Parametric Technology Corporation.
- [9] St. Michel, N., “Force Multiplier in a Micromechanical Silicon Oscillating Accelerometer.” Master’s Thesis, Massachusetts Institute of Technology, June 2000.

- [10] Strogatz, S., Stewart, I., "Coupled Oscillations and Biological Synchronization," Scientific American, Dec. 1993, pp. 68-75.
- [11] Weaver, W., Timoshenko, S.P., Young D.H., *Vibration Problems in Engineering*, Chapter 5.17. John Wiley and Sons., 1990.
- [12] Williams, J., *Fundamentals of Applied Dynamics*. Chapter 8-4. John Wiley and Sons, Inc., 1996.